İSTANBUL TECHNICAL UNIVERSITY ★ INSTITUTE OF SCIENCE AND TECHNOLOGY

SOME PHYSICAL EFFECTS OF BLACK HOLES:
THEORY AND OBSERVATIONS

M.Sc. Thesis by
Pamir TALAZAN

Department : Physics Engineering

Programme : Physics Engineering

JUNE 2009

İSTANBUL TECHNICAL UNIVERSITY ★ INSTITUTE OF SCIENCE AND TECHNOLOGY

SOME PHYSICAL EFFECTS OF BLACK HOLES:
THEORY AND OBSERVATIONS

M.Sc. Thesis by
Pamir TALAZAN
(509061111)

Date of submission	:	**4 May 2009**
Date of defence examination	:	**2 June 2009**

Supervisor (Chairman)	:	**Prof. Dr. Ömer Faruk DAYI (ITU)**
CoSupervisor	:	**Assoc. Prof. Dr. Alikram NUHBALAOĞLU (FGI)**
Members of the Examining Committee	:	**Prof. Dr. Tekin DERELİ (KU)**
		Assist. Prof. Dr. A. Savaş ARAPOĞLU (ITU)
		Assist. Prof. Dr. Aybike ÖZER (ITU)

JUNE 2009

İSTANBUL TEKNİK ÜNİVERSİTESİ ★ FEN BİLİMLERİ ENSTİTÜSÜ

KARA DELİKLERİN BAZI FİZİKSEL ETKİLERİ:

TEORİ VE GÖZLEMLER

YÜKSEK LİSANS TEZİ
Pamir TALAZAN
(509061111)

Tezin Enstitüye Verildiği Tarih	:	**4 Mayıs 2009**
Tezin Savunulduğu Tarih	:	**2 Haziran 2009**

Tez Danışmanı	:	**Prof. Dr. Ömer Faruk DAYI (İTÜ)**
Eş Danışman	:	**Doç. Dr. Alikram NUHBALAOĞLU (FGE)**
Diğer Jüri Üyeleri	:	**Prof. Dr. Tekin DERELİ (KÜ)**
		Yard. Doç. Dr. A. Savaş ARAPOĞLU (İTÜ)
		Yard. Doç. Dr. Aybike ÖZER (İTÜ)

HAZİRAN 2009

FOREWORD

First, I want to thank Alikram Nuhbalaoğlu for giving me the problem for my thesis and for his patient and careful supervision of my work at all stages. I learned a lot from his deep insight of the subject and I am strongly influenced by his scientific intuition.

I would also like to thank Ömer Faruk Dayı for his understanding and support.

Also, I like to thank all my loved ones and friends for taking part in my life and influencing it in any way.

Finally, I would like to thank Prof. Dr. Osman Teoman Turgut for his encouragement and support, and all the members and workers of TÜBİTAK - Feza Gürsey Institute for creating the most peaceful working environment one can hope.

TABLE OF CONTENTS

ABBREVIATIONS

QPO	:	Quasi-periodic Oscillation
ISCO	:	Innermost Stable Circular Orbit
BH	:	Black Hole
AdS	:	Anti-de Sitter
CFT	:	Conformal Field Theory
ADD	:	Arkani-Hamed-Dimopoulos-Dvali
RS	:	Randall-Sundrum
ADM	:	Arnowitt-Deser-Misner

x

LIST OF TABLES

LIST OF FIGURES

LIST OF SYMBOLES

$\mathbf{M}_\odot$:   Solar mass

$\mathbf{M}_\odot$	:	Solar mass
$\mathbf{a}$	:	Angular momentum per unit mass
β	:	Tidal charge of braneworld BH
$\mathbf{c}$	:	Speed of light
$\mathbf{G}$	:	Gravitational constant
$\mathbf{R}_{\mu\nu\lambda\tau}$	:	Riemann tensor
$\mathbf{C_{ABCD}}$	:	Five-dimensional Weyl tensor
$\mathbf{g}_{\mu\nu}$	:	Metric tensor
$\mathbf{T}_{\mu\nu}$	:	Energy-momentum tensor
$\mathbf{K}_{\mu\nu}$	:	Killing tensor
$\mathbf{R_{ij}}$	:	Ricci tensor
$\mathbf{E_{ij}}$	:	Traceless "electric part" of Weyl tensor
$\mathbf{R}$	:	Ricci scalar
$\mathbf{\Gamma}^\mu_{\alpha\beta}$	:	Christoffel symbol
$\mathbf{\Omega}_0$	:	Orbital frequency
$\mathbf{\Omega}_s$	:	Kepler frequency
$\mathbf{\Omega}_r$	:	Radial epicyclic frequency
$\mathbf{\Omega}_\theta$	:	Vertical epicyclic frequency
$\mathbf{\Omega}_{PP}$	:	Periastron precession frequency
$\mathbf{\Omega}_{LT}$	:	Lense-Thirring precession frequency
$\mathbf{r}_+$	:	Radii of event horizon
$\mathbf{r_{ph}}$	:	Radii of photon orbit
$\mathbf{r_{ms}}$	:	Radii of ISCO
$\mathbf{r_l}$	:	Characteristic length scale in BH spacetime
$\nu_\mathbf{l}$	:	Characteristic frequency scale in BH spacetime

SOME PHYSICAL EFFECTS OF BLACK HOLES: THEORY AND OBSERVATIONS

SUMMARY

Black holes are one of the most exciting and fascinating objects of study in modern theoretical physics and astrophysics. In this thesis, we study some observable effects of black holes in general relativity and braneworld gravity. We begin with an overview of basic properties of these black holes and modern observations of X-ray binary systems, which are believed to harbor a black hole. Next, we study the theory of motion of test particles in terms of three fundamental frequencies, earlier developed by Aliev and Gal'tsov, and present analytical expressions for the orbital and epicyclic frequencies in the field of a Kerr black hole and a rotating braneworld black hole with a tidal charge in the Randall-Sundrum braneworld scenario. The tidal charge transmits the signature of an extra spacelike dimension into our observable world. First, we perform a detailed numerical analysis of these frequencies for the Kerr black hole and show that, at some particular stable circular orbits, the values of the radial and vertical epicyclic frequencies are in good qualitative agreement with the frequencies of twin peaks quasi-periodic oscillations (QPOs) detected in some black hole binaries. We then proceed with a numerical analysis of the epicyclic frequencies for the braneworld black hole and find that, unlike the case of the positive tidal charge, the existence of the negative tidal charge appears to be in agreement with modern observations of black holes. Finally, we study the relativistic precession effects (*periastron* and *frame-dragging*) in the field of both these black holes. We show that for sufficiently fast rotation of the black holes, the precession frequencies at some characteristic radii exhibit $3:1$ and $2:1$ ratios. We also show that it is the rotation parameter that plays a crucial role to distinguish between a Kerr black hole and a rotating braneworld black hole. In the latter case, the rotation parameter obeys the inequality $a > M$.

KARA DELİKLERİN BAZI FİZİKSEL ETKİLERİ: TEORİ VE GÖZLEMLER

ÖZET

Kara delikler, modern teorik fiziğin ve astrofiziğin en heyecan verici ve ilginç çalışma alanlarından biridir. Bu tezde genel görelilik ve zarlar üzerinde evren teorilerinde kara deliklerin bazı gözlemsel etkileri araştırılmaktadır. Öncelikle, bu kara deliklerin temel özellikleri ve kara delik barındırdığı düşünülen X-ışını ikili yıldız sistemlerinin modern gözlemleri tasvir edilmektedir. Ardından, önceden Aliev ve Gal'tsov tarafından geliştirilmiş olan test parçacıkların üç temel frekans cinsinden hareket teorisi incelenerek, Kerr ve "tidal" yüklü zarlar üzerinde Randall-Sundrum evreni senaryosunda dönen kara delikler için yörüngesel ve episiklik frekansların analitik ifadeleri elde edilmektedir. Tidal yük, ek uzaysal boyutun fiziksel imzasını bizim gözlenebilir dünyamıza taşımaktadır. İlk olarak, bu frekansların bazı özel dairesel yörüngelerde detaylı sayısal analizleri yapılarak, radyal ve dikey episiklik frekansların, kara delik barındıran bazı ikili yıldız sistemlerinde gözlemlenmiş olan ikiz tepeli kuazi-periyodik salınımların frekanslarıyla niteliksel olarak uyumlu olduğu gösterilmektedir. Daha sonra, zarlar üzerinde evren teorisinde dönen kara delik için episiklik frekansların sayısal analizleri yapılarak, pozitif tidal yük durumundan farklı olarak, negatif tidal yükün varoluşunun kara deliklerin modern gözlemleriyle uyum içinde olabileceği ortaya konulmaktadır. Son olarak, her iki tür kara deliğin alanında iki rölativistik olayın, periastron ve çerçeve-sürükleme devinmesi, incelenmektedir. Kara deliklerin yeterince hızlı dönme durumunda ve belirli yörüngeler için, devinme frekanslarının, $3:1$ ve $2:1$ oranlarında olduğu gösterilmektedir. Bu bağlamda, dönen Kerr ve zarlar üzerinde kara deliklerin birbirinden ayrılması açısından dönme parametresinin kritik bir rol oynadığı ortaya konulmaktadır ve zarlar üzerinde kara delikler için dönme parametresinin $a > M$ olabileceği vurgulanmaktadır.

1. INTRODUCTION

Nowadays, the idea of a black hole is regarded as being one of the most fundamental ideas in modern theoretical physics and it occupies a central place in all theories of gravity formulated in various spacetime dimensions. It is a truly remarkable fact that all these theories, from general relativity to supergravity and string theory, provide an elegant mathematical description of this idea in terms of exact solutions to the corresponding field equations. These solutions are of great significance for many reasons: After all, they shed light on the nature of gravity theories themselves, facilitating the study of their structure and dynamics, playing the role of theoretical "guide-laboratories" to figure out the novel consequences of these theories, such as the AdS/CFT correspondence in string theory [1–7]. It is also a striking fact that modern astronomical observations provide compelling and overwhelming evidence for the existence of black holes in the real universe.

In the light of all these developments, this thesis is devoted to the following group of issues:

1. The description of the current theoretical status of black holes in general relativity and braneworld gravity as well as modern observations of black holes in X-ray binary systems.

2. The motion of test particles around Kerr black holes in terms of three fundamental frequencies: the *orbital* frequency, the radial and the vertical *epicyclic* frequencies. The exploration of possible appearances of these frequencies in astrophysical black hole systems.

3. The signature of the fifth dimension in the motion of test particles around rotating braneworld black holes. The full numerical analysis of the orbital and epicyclic frequencies and their astrophysical consequences.

4. The study of relativistic precessions (periastron and frame-dragging) and their observable effects in the field of both rotating Kerr and braneworld black holes.

1.1 Black Holes in General Relativity

General relativity admits a unique family of stationary black hole solutions, which turns out to be crucial for understanding its nature and the occurrence of spacetime singularities [6,7]. Furthermore, these solutions possess a number of striking properties. Among them are the properties of stability, spherical topology of the horizon, hidden symmetries and integrability of geodesics, superradiance and quantum evaporation [8–13] (see also books [14,15]). Apart from their obvious and deep physical significance, these properties pave the way for astrophysical implications of general relativity in the regime of strong gravity and constitute a firm ground for the search of black holes in the universe.

An astrophysical black hole is supposed to be likely described by an exact stationary solution of the Einstein field equations discovered in 1963 by R. Kerr [16]. This solution is uniquely characterized by two physical parameters: The mass and the angular momentum. In addition to its global time-translational and rotational symmetries, this solution also possesses hidden symmetries, generated by a second rank Killing tensor [17]. Therefore, it becomes possible to achieve a complete separation of variables both in the Hamilton-Jacobi equation for geodesics [12] and in equations for scalar, electromagnetic and gravitational perturbations [18]. This in turn opens up the way for analytical studies of the behavior of particles and waves in the vicinity of Kerr black holes. For example, the complete integrability of geodesic motion in the Kerr metric allows to calculate the observable orbits of test particles. Bardeen *et al.* [19] gave an analytical description of these orbits for the circular motion. In particular, they calculated precisely the regions for the existence and stability of these orbits. The binding energy of the innermost stable circular orbit (ISCO) determines the maximum amount of energy, which is radiated away by a test particle approaching this orbit. This energy for a maximally rotating Kerr black hole can attain nearly 42% of the particle rest-mass energy, whereas for a static Schwarzschild black hole it is about 6%. The high efficiency of this process constitutes a firm basis for invoking

the idea of an accretion disk around a black hole to explain the enormous energy output observed in both X-ray binary systems and active galactic nuclei (see [20] and references therein for details).

1.2 Black Holes in Braneworld Gravity

Black holes in braneworlds are higher-dimensional objects. The braneworld idea is a leading endeavor to reconcile the properties of gravity in higher dimensions with those of four-dimensional gravity [21–24]. A braneworld is a four-dimensional slice of a higher-dimensional space, on which our physical world resides. In other words, all matter fields are supposed to be localized on the slice (3-brane) except gravity. Gravity being dynamics of the spacetime itself is free to act in all dimensions. Therefore, exploring the behavior of gravity in braneworld scenarios one may provide a way of tackling extra unseen dimensions. In this regard, black holes in these scenarios might have played an indispensable role.

The first striking confirmation of this idea has appeared in Arkani-Hamed-Dimopoulos-Dvali (ADD) braneworld scenario [21], where the large size of the extra spatial dimensions (compared to the Planckian length $\sim 10^{-33}cm$), renders the scale of quantum gravity to be as lower as TeV-energy scales, thereby opening up the possibility for the formation of mini black holes at these scales. Such black holes would carry the imprints of extra dimensions and their detection at high-energy experiments would be a great triumph for gravitational physics in higher dimensions [25,26]. Another intriguing braneworld scenario with a warped and infinite extra dimension was proposed by Randall and Sundrum (RS) [24], which in the low energy limit, to high enough accuracy, supports the properties of four-dimensional Einstein's gravity on the brane [27,28]. The similar effective field equations on the 3-brane, imprinted by a five-dimensional gravity with a second order Gauss-Bonnet term, were obtained in [29,30]. Therefore, it is natural to expect the formation of black holes in this braneworld scenario.

A complete description of black holes in the braneworld scenarios is a challenging and thorny problem. There have been several approaches to the description of these black holes: The first approach is built up on invoking the classical

higher-dimensional black hole solutions found by Tangherlini [31] for static black holes and by Myers and Perry [32] for rotating black holes. These solutions generalize the well-known Schwarzschild, Reissner-Nordström and Kerr solutions to arbitrary spacetime dimensions. The charged versions of the Myers-Perry solution are discussed in papers [33–36].

From the physical point of view, it is clear that if a black hole on the brane is small enough compared to the size of the extra dimensions, it would behave as a "generic" higher-dimensional object, equally affected by all the spacetime dimensions. These black holes can be effectively described using the Tangherlini or Myers-Perry solutions. However, if the size of a black hole on the brane is much larger than that of the extra dimensions, the black hole can be thought of as an effectively four-dimensional object with some finite part of the horizon, leaking into the bulk space. Such black holes could be formed as a result of the gravitational collapse of matter on the brane. Chamblin *et al.* [37] suggested to describe these black holes by the usual Schwarzschild solution on the Randall-Sundrum brane, which from the five-dimensional point of view would look like a *black string*. The main drawback of the black string solution is that it suffers from curvature singularities propagating along the extra dimension.

Another approach to the braneworld black holes is to specify (postulate) the spacetime metric form on the brane and solve the effective gravitational field equations [27,28]. It gives a Reissner-Nordstrom type solution for static black holes [38] and a Kerr-Newman type solution for rotating black holes on the brane [39]. These solutions carry a *tidal* charge instead of an electric charge, thereby transmitting the gravitational signature of the bulk space into the four-dimensional world on the brane. Further developments in this direction can be found in [40–53].

1.3 Observations of Black Holes

Modern astronomical observations carried out in all bands of the electromagnetic spectrum have revealed dozens of compact and dark objects in binary stellar systems. These objects are reliably identified as black holes. Solid observational

data also point in favor of the presence of supermassive black holes at the centers of most galaxies, including our Milky Way Galaxy. Below, we focus only on stellar mass black holes.

1.3.1 Stellar mass black holes

The first real example of a black hole was identified with an unusual X-ray source discovered in the binary Cygnus X-1 at the beginning of the 1970s [54]. The most attractive features of this source are its persistently bright character in X-rays and the presence of the widest range of temporal variability in the spectrum. The companion star is a massive optical star of spectral class O/B (hot supergiant). In order to identify this X-ray source as a black hole, it is *crucial* to determine its mass from the observable parameters of the binary.

The observable parameters of a binary, the orbital period P_{orb} and the Doppler velocity of the companion star along the line of sight $K_c = v \sin i$, where i is the inclination angle of the orbital plane, are determined from the analysis of its optical light curve. With these parameters, one can evaluate the "mass function" of the binary by the formula

$$f(M) = \frac{K_c^3 P_{orb}}{2\pi G} = \frac{M \sin^3 i}{(1 + M_c/M)^2}, \tag{1.1}$$

where M_c is the mass of the companion star, M is the mass of unseen compact object and G is the gravitational constant [20].

It can be argued that the mass function gives a lower bound for the mass of the compact object. It is important to note that the evaluation of the mass function requires an independent estimate of the mass M_c and for its large values the factor $(1 + M_c/M)^2$ in the denominator causes additional uncertainties. However, the opposite occurs for binaries with low-mass companion stars. The mass of the X-ray source in Cygnus X-1 has been measured very accurately and found to be $M \geq 6M_\odot$, where $M_\odot$ is the mass of the Sun. This value well exceeds the limiting stable mass for a neutron star in general relativity $M \geq 3M_\odot$, confirming that X-ray source in Cygnus X-1 is a black hole [20].

A new stage in the search for black holes has come with the discovery of a rather dramatic transient X-ray source in the binary system GRS 1915 + 105 in the

constellation of Aquila [55]. This source has a low-mass normal star companion and flares up to maximum X-ray luminosity of order 10^{40} erg/s. Furthermore, it also shows very strong and wide X-ray variability patterns as well as very powerful, relativistic radio jets. For this reason, this X-ray source is also called a "microquasar". Measuring the mass of the dark companion has shown that it is a black hole of mass $M \simeq (10\text{--}18)M_\odot$. Another microquasar with the similar properties was discovered in low-mass X-ray binary GRO J1655-40 [56] in the constellation of Scorpius, where the dark companion is identified as a black hole of mass $M \simeq 7M_\odot$.

The number of X-ray binary systems harboring black holes is constantly growing. Today at least twenty confirmed black holes and twenty black hole candidates are known. A comprehensive description of the observational properties of these black holes can be found in recent review papers [57,58]. The list of twenty X-ray binaries with black holes is given in Table 1.1.

Table 1.1: Dynamically-confirmed black holes (from R. A. Remillard and J. E. McClintock (2006)).

Coordinate Name	Common Name/Prefix	Spec.	P_{orb} (hr)	f(M) ($M_\odot$)	M_1 ($M_\odot$)
0422+32	(GRO J)	M2V	5.1	1.19±0.02	3.7–5.0
0538–641	LMC X–3	B3V	40.9	2.3±0.3	5.9–9.2
0540–697	LMC X–1	O7III	93.8	0.13±0.05	4.0–10.0
0620–003	(A)	K4V	7.8	2.72±0.06	8.7–12.9
1009–45	**(GRS)**	**K7/M0V**	**6.8**	**3.17±0.12**	**3.6–4.7**
1118+480	**(XTE J)**	**K5/M0V**	**4.1**	**6.1±0.3**	**6.5–7.2**
1124–684	**Nova Mus 91**	**K3/K5V**	**10.4**	**3.01±0.15**	**6.5–8.2**
1354–64	**(GS)**	**GIV**	**61.1**	**5.75±0.30**	**–**
1543–475	(4U)	A2V	26.8	0.25±0.01	8.4–10.4
1550–564	**(XTE J)**	**G8/K8IV**	**37.0**	**6.86±0.71**	**8.4–10.8**
1650–500	(XTE J)	K4V	7.7	2.73±0.56	–
1655–40	(GRO J)	F3/F5IV	62.9	2.73±0.09	6.0–6.6
1659–487	**GX 339–4**	**–**	**42.1**	**5.8±0.5**	**–**
1705–250	**Nova Oph 77**	**K3/7V**	**12.5**	**4.86±0.13**	**5.6–8.3**
1819.3–2525	**V4641 Sgr**	**B9III**	**67.6**	**3.13±0.13**	**6.8–7.4**
1859+226	**(XTE J)**	**–**	**9.2**	**7.4±1.1**	**7.6–12.0**
1915+105	**(GRS)**	**K/MIII**	**804.0**	**9.5±3.0**	**10.0–18.0**
1956+350	Cyg X–1	O9.7Iab	134.4	0.244±0.005	6.8–13.3
2000+251	**(GS)**	**K3/K7V**	**8.3**	**5.01±0.12**	**7.1–7.8**
2023+338	**V404 Cyg**	**K0III**	**155.3**	**6.08±0.06**	**10.1–13.4**

We note that only three of these sources are persistently bright in X-rays: one galactic source, Cygnus X-1, and two extragalactic sources, LMC X-1, LMC X-3. The remaining seventeen sources are transient in X-rays. The most crucial point in identification of these sources as black holes is the determination of their masses, according to the formula given in (1.1). For these twenty black holes there exists very strong dynamical evidence for measuring their masses and therefore, they are called *dynamically-confirmed* black holes.

It is curious to note that in some cases (bolded in the table) the mass function itself exceeds the maximum mass $M \simeq 3M_\odot$ predicted for a neutron star. It is also important to note that, in some cases, there exists strong evidence for the existence of the event horizons as well (see [57] and references therein), thereby confirming that these sources are true black holes. Furthermore, in some X-ray binaries with black holes, high-frequency *quasiperiodic oscillations* with a single frequency, or with a pair of characteristic frequencies have been observed [57,59, 60]. The appearance of such frequencies in the X-ray spectra are of fundamental importance as they are supposed to be determined by strong gravity effects. We pass now to the description of these oscillations.

1.3.2 Quasi-periodic oscillations

As we have described above, astrophysical black holes are identified as massive X-ray sources. As is known, in the classic sense black holes do not radiate anything. That is, they are completely invisible. However, in the real universe black holes become visible due to a powerful energy output from their vicinity. Gravitationally interacting with the surrounding medium, a black hole captures ambient matter. This matter spirals in nearly Keplerian orbits towards the innermost stable circular orbit, forming an accretion disk around the black hole.

In the inner region of the accretion disk, temperatures attain so high values, $T \geq 10^7$ K, that a powerful energy release occurs in X-rays that makes the black hole visible. The accretion flow has a turbulent nature that causes stochastic variability on a wide-range time scales. The rapid variations are of particular importance as they are generated in the strong gravity regime near black holes.

Recent observations of black hole binaries on many occasions have revealed finite-width peaks in the X-ray spectra. These peaks are believed to be signatures of quasi-periodic oscillations (QPOs) of the black hole accretion disk [58]. Remarkably, besides low-frequency QPOs (0.1 - 30 Hz), high-frequency QPOs (> 40 Hz) have also been detected in a number of cases [57,59,60]. Furthermore, it turned out that these frequencies are almost stable to variations of X-ray flux and scale with inverse mass of the black hole. This observational fact is a strong indication that the high-frequency QPOs are largely determined by the properties of relativistic gravity. These frequencies offer a new way for measuring the angular momentum of black holes (see a review paper [61] and references therein).

At present, high-frequency QPOs have been seen in five black hole binaries and in two binaries containing black hole candidates. In four sources, two peaks of QPOs were detected (though not always simultaneously). The frequencies of these QPOs are: (300, 450 Hz) for X-ray binary GRO J1655-40; (113, 168 Hz) for X-ray binary GRS 1915 + 105; (184, 276 Hz) for X-ray binary XTE J1550-564 and (165, 241 Hz) for X-ray binary H 1743-322, which contains a black hole candidate. It is easy to check that these twin frequencies are nearly in a 2:3 ratio. We note that the source GRS 1915 + 105 has exhibited another pair of high-frequency QPOs (41, 67 Hz) which are not in a 2:3 ratio and also a pair (164, 328 Hz), which is in a 1:2 ratio. The remaining three sources have shown (at least till now) only single oscillations: In XTE J1650-500 (250 Hz); XTE J1859+226 (190Hz) and in 4 U 1630-47 (184 Hz). The latter source is a black hole candidate(see [57,58] and references therein for details). In Figure 1.1, we present the list of the X-ray binaries with high-frequency QPOs. The solid patterns correspond to the energy range 13-30 keV, whereas the dashed patterns were obtained for the energy range 2-30 keV.

We emphasize once again that all these high-frequency QPOs exhibit, to high enough accuracy, stability in frequency with respect to considerable changes of the luminosity. This is a crucial feature that does not occur for high-frequency QPOs observed in accreting neutron stars. Another striking feature of these high-frequency QPOs is that they can be related to the fundamental epicyclic frequencies of test particles in the spacetime of rotating black holes, which for
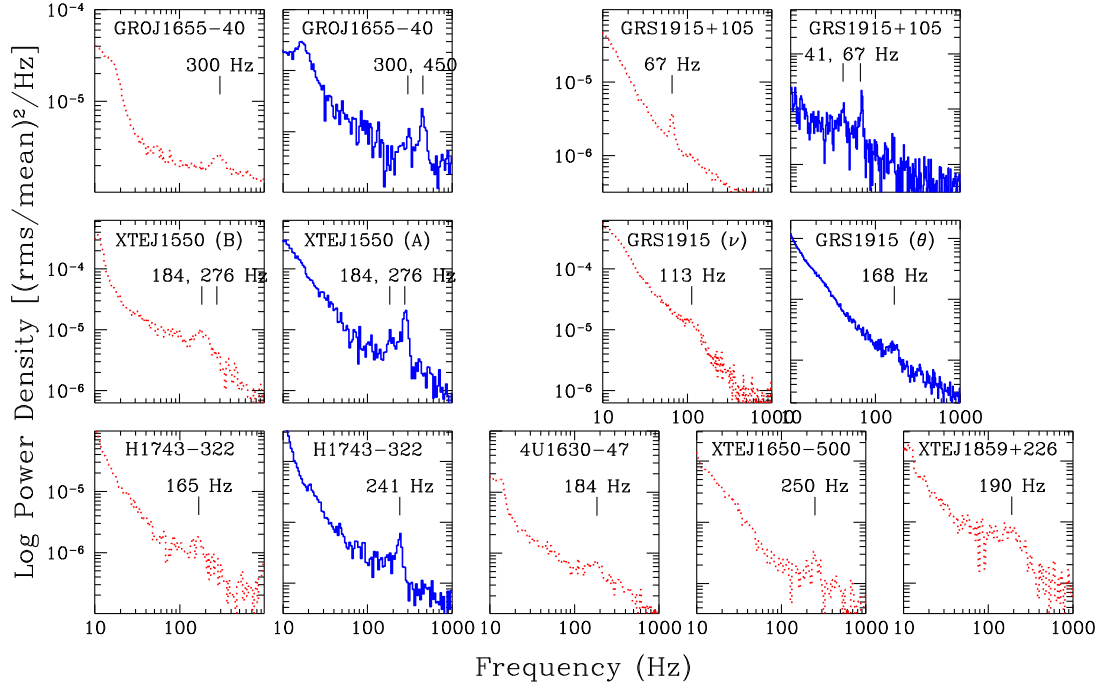
Figure 1.1: High-frequency QPOs in X-ray binaries (from R. A. Remillard and J. E. McClintock (2006)).

the first time were calculated in 1981 by Aliev and Gal'tsov [62]. This fact lies at the roots of many theoretical models of the high-frequency QPOs discussed in the literature over the last years [63–65]. See also recent papers [42,43,66,67]. However, it is also worth noting that at present a complete and widely accepted model for the QPOs phenomenon still needs to be constructed.

1.4 New Perspectives and Thesis Outline

The advances in observations of black holes raise, among many others, a simple and natural question: *Are the observed black holes exact prototypes of those predicted by general relativity*?

Today this question is largely open as observations of high-frequency QPOs as well as relativistically-broadened Fe Kα line formed near the ISCO have been carried out near the limiting sensitivity of X-ray detectors.

Future cosmic missions with much more sensitive X-ray detectors on aboard will certainly provide crucial data for more precise measurements of the observable features of black holes, such as the angular momentum and the radius of ISCO etc. Of course, *it may happen that the observational data confront with the predictions of general relativity*. This perspective seems to be very exciting and greatly

stimulates theoretical studies of the observable properties of black holes beyond general relativity both in four and higher-dimensional spacetimes [68,69].

It is this perspective that was the baseline and the main motivation for the study of rotating black holes in this thesis. We consider two examples of the black holes: (i) the usual Kerr black holes in general relativity, (ii) rotating black holes in braneworld gravity. In the framework of the theory of cyclic and epicyclic motions of test particles, developed earlier in [62,70–72], we explore the observable effects of these black holes.

The thesis is organized as follows. In Chapter 2 we give a brief description of the properties of a Kerr black hole in general relativity, focusing mainly on its event horizon and ergosphere structures. Next, we describe the circular and quasi-circular motions of test particles in terms of three fundamental frequencies: the orbital frequency and the frequencies of the epicyclic motion in the radial and vertical directions. We perform a detailed numerical analysis of these frequencies both at ISCOs and beyond as well as at some particular radii, for which the radial epicyclic frequency attains its highest value. In Chapter 3 we describe the properties of a rotating braneworld black hole which may carry both positive and negative tidal charges. For the negative tidal charge, the event horizon and the ergosphere of this black hole appear to be significantly different from those of the usual Kerr-Newman black hole in general relativity. Here we obtain analytical expressions for the fundamental frequencies of the test particle motion and perform their full numerical analysis for both positive and negative values of the tidal charge. We focus on orbits, where the radial epicyclic frequency reaches its maximum value and compare the results with those obtained for a Kerr black hole. We also point out the distinguished effects of the negative tidal charge and discuss their observational signatures. Finally, we discuss two relativistic effects, periastron and frame-dragging precessions, around rotating black holes with zero and nonzero (negative) tidal charge.

2. ROTATING KERR BLACK HOLES

The most general stationary black hole solution in general relativity is given by the Kerr-Newman metric [15,73], which satisfies the coupled system of Einstein-Maxwell equations. This solution gives a unique description of the spacetime of rotating and electrically charged black holes. Though the presence of the electric charge is of great interest from the theoretical point of view, in realistic astrophysical situations the charge is usually negligible. Therefore, in the astrophysical sense, it is most fitting to consider rotating black holes with zero electric charge which are described by the Kerr metric.

2.1 The Kerr Metric and Its Properties

This metric is a unique stationary solution to the Einstein field equations in four dimensional spacetime and it was found by New Zealand mathematician Roy Kerr [16]. The black hole nature of this solution becomes immediately evident when one explores its form written in the Boyer-Lindquist coordinates [15]. In these coordinates, the metric is given by

$$ds^2 = -\frac{\Delta}{\Sigma}\left(dt - a\sin^2\theta\,d\phi\right)^2 + \Sigma\left(\frac{dr^2}{\Delta} + d\theta^2\right) + \frac{\sin^2\theta}{\Sigma}\left[adt - (r^2 + a^2)\,d\phi\right]^2, \quad \textbf{(2.1)}$$

where the metric functions

$$\Delta = r^2 + a^2 - 2Mr,$$

$$\textbf{(2.2)}$$

$$\Sigma = r^2 + a^2\cos^2\theta$$

and M is the mass, a is the rotation parameter or the angular momentum per unit mass, $a = J/M$. For $a = 0$, this metric reduces to the Schwarzschild solution. We note that for the Kerr-Newman metric we have the same expression as in (2.1), but the metric function Δ is replaced by

$$\Delta = r^2 + a^2 - 2Mr + Q^2, \qquad \textbf{(2.3)}$$

where Q is the electric charge.

Looking at the metric components in (2.1), we immediately note that they do not depend on t and ϕ. That is, the time coordinate t and the azimuthal coordinate ϕ are ignorable coordinates. In other words, the Kerr metric admits global time-translational and rotational symmetries (*isometries*). Mathematically, these isometries are described by two commuting Killing vectors

$$\xi_{(t)} = \frac{\partial}{\partial t},$$
$$\xi_{(\phi)} = \frac{\partial}{\partial \phi},$$

(2.4)

which satisfy the Killing equation

$$\nabla_{(\mu}\xi_{\nu)} = 0,$$

(2.5)

where ∇ denotes a covariant derivative operator with respect to the metric (2.1) and round parentheses here and in the following denote symmetrization over the indices enclosed.

It is easy to see that the Kerr metric becomes singular in two cases; $\Delta = 0$ and $\Sigma = 0$. The most convenient way to figure out the nature of these singularities is the calculation of the curvature invariant for this metric. Having done this, we find that

$$R_{\mu\nu\lambda\tau}R^{\mu\nu\lambda\tau} = \frac{48M^2(2r^2 - \Sigma)(\Sigma^2 - 16r^2a^2\cos^2\theta)}{\Sigma^6}.$$

(2.6)

It follows that this expression diverges at $\Sigma = 0$, i.e. the singularity along this surface is the only curvature singularity. This also shows that the singularity at the surface $\Delta = 0$ is a coordinate singularity of the Kerr metric, which can be assigned a clear physical meaning. Indeed, one can show that the equation

$$\Delta = r^2 + a^2 - 2Mr = 0,$$

(2.7)

describes a null surface. The largest root of this equation

$$r_+ = M + \sqrt{M^2 - a^2}$$

(2.8)

corresponds to the radius of a region in the spacetime, which is called *the event horizon*. From the geometrical point of view, the event horizon is a surface of zero expansion for outgoing null geodesics, which are orthogonal to this surface.

12

That is, the square of the normal vector $n_\mu = \partial_\mu r$ to this surface must vanish. This gives us the condition $g^{rr} = 0$, which is equivalent to that given in (2.7).

In an alternative approach, the existence of the event horizon in the Kerr metric can be justified by exploring the isometries of the horizon geometry. For this purpose, it is useful to introduce a family of static (locally nonrotating) observers, whose velocity vector u^μ is orthogonal to the surface $t = \text{const}$. This means that for these observers we have the equations

$$u^r = u^\theta = 0, \quad u \cdot \xi_{(\phi)} = 0, \tag{2.9}$$

which give the following expression for their coordinate angular velocity

$$\Omega = -\frac{g_{t\phi}}{g_{\phi\phi}} = \frac{a\left(r^2 + a^2 - \Delta\right)}{\left(r^2 + a^2\right)^2 - \Delta a^2 \sin^2\theta} . \tag{2.10}$$

We see that this expression is finite at $\Delta = 0$ and approaches its limiting constant value

$$\Omega_H = \frac{a}{r_+^2 + a^2} . \tag{2.11}$$

Next, following the Hawking idea [10,11] one can define a new vector field

$$\chi = \xi_{(t)} + \Omega_H \, \xi_{(\phi)}, \tag{2.12}$$

which certainly satisfies the Killing equation (2.5) as the quantity Ω_H is constant. It is straightforward to show that the square of this new Killing vector vanishes at $\Delta = 0$. That is, the Killing vector describes the isometries of the null surface $r = r_+$ and it is tangent to the null geodesics, which rotate along this surface with an angular velocity Ω_H. Thus, the null surface at $r = r_+$ acts as an event horizon to a distant observer. *The existence of the event horizon is the most striking fact towards the identification of the Kerr spacetime as containing a rotating black hole.*

It is important to note that the event horizon, as it follows from equation (2.8), exists provided that

$$a \leq M. \tag{2.13}$$

This is the requirement of a "Cosmic Censor" (the absence of naked singularities), which states that a rotating black hole in general relativity must possess an angular momentum not exceeding its mass.

Another striking feature of the Kerr metric stems from the fact that the norm of the timelike Killing vector $\xi_{(t)}$ does not vanish on the horizon. From the equation

$$\xi_{(t)} \cdot \xi_{(t)} = g_{tt} = 0, \tag{2.14}$$

we find that

$$r_0 = M + \sqrt{M^2 - a^2 \cos^2 \theta}, \tag{2.15}$$

where r_0 is the largest root of this equation. It easy to see that this surface lies outside the horizon and therefore, this region does communicate with the outside world. This region is called the *ergosphere* of the Kerr metric. Inside the ergosphere the timelike Killing vector becomes spacelike, which means that all observers here must necessarily corotate with the black hole. *The physical significance of the ergosphere is that it allows the extraction of the rotational energy from the Kerr black holes in the Penrose-type processes* (see, for instance [14]).

2.2 The Motion of Test Particles

The test particles in the spacetime of a Kerr black hole move along the geodesics of this spacetime. The global isometries of the Kerr metric described by the Killing vectors (2.4) immediately result in two constants of motion, corresponding to the total energy E and angular momentum L (along black hole's rotation axis) of a test particle. However, the Kerr spacetime, in addition to its global symmetries, also admits the hidden symmetries which are generated by a second rank Killing tensor $K_{\mu\nu}$. Solving explicitly the Killing equation

$$\nabla_{(\lambda} K_{\mu\nu)} = 0, \tag{2.16}$$

we find that the nonvanishing components of this tensor are given by [17]

$$K_{\mu\nu} dx^\mu dx^\nu = \frac{\Delta a^2 \cos^2 \theta}{\Sigma} \left(dt - a \sin^2 \theta d\phi \right)^2 - \frac{\Sigma a^2 \cos^2 \theta}{\Delta} dr^2$$
$$+ \Sigma r^2 d\theta^2 + \frac{r^2 \sin^2 \theta}{\Sigma} \left[adt - (r^2 + a^2) d\phi \right]^2. \tag{2.17}$$

The Killing tensor provides us with a new, quadratic in the particle 4-momentum, constant of motion $K = K_{\mu\nu} p^\mu p^\nu$. As it follows from equation (2.16), another obvious Killing tensor is the spacetime metric $g_{\mu\nu}$ itself that gives the mass of

the particle $-m^2 = g_{\mu\nu}p^\mu p^\nu$. All together, these constants of motion guarantee a complete separation of variables in the Hamilton-Jacobi equation for geodesics. This was explicitly shown in 1968 by Carter [12], who achieved the separation of variables by substituting the expansion of the action

$$S = \frac{1}{2}m^2\lambda - Et + L\phi + S_r(r) + S_\theta(\theta) \tag{2.18}$$

into the Hamilton-Jacobi equation

$$\frac{\partial S}{\partial \lambda} + \frac{1}{2}g^{\mu\nu}\frac{\partial S}{\partial x^\mu}\frac{\partial S}{\partial x^\nu} = 0, \tag{2.19}$$

where λ is an affine parameter.

In some cases, especially when studying the equatorial and quasi-equatorial motions, it is convenient to invoke the geodesic equation

$$\frac{d^2 x^\mu}{ds^2} + \Gamma^\mu_{\alpha\beta}\frac{dx^\alpha}{ds}\frac{dx^\beta}{ds} = 0, \tag{2.20}$$

where the parameter s can be thought of as the proper time along the geodesic curves. Using the geodesic equation one can employ the method of successive approximations and describe the motion of test particles in an arbitrary stationary and axially symmetric spacetime in terms of *three fundamental frequencies*. In this approach, the circular motion in the equatorial plane is described at the zeroth-order approximation and is characterized by the usual orbital frequency [19]. Small perturbations about circular orbits lead to the quasi-circular (epicyclic) motion which, at the first-order approximation, amounts to two decoupled oscillations in the radial and vertical directions. In 1981, Aliev and Gal'tsov calculated the frequencies of these oscillations in the most general case of the Kerr-Newman field and charged test particles [62]. The authors have also put forward the idea that at higher-order approximations these oscillations may couple, resulting in nonlinear resonance phenomena. In 1986, the epicyclic frequencies in the Kerr field were used to develop the theory of multi-resonant interaction of test particles and electromagnetic waves in the vicinity of rotating black holes [70] (see also [71] and a review paper [72]). Later on, the expressions for the frequencies of radial and vertical oscillations in the Kerr field were rederived in [74,75] and have been studied in many physical and astrophysical

15

contexts (for instance, see [42,43,63,64,76] and references therein). Below, closely following the works of [62,70–72], we describe the cyclic and epicyclic motions of the test particles in the Kerr field.

2.3 Circular Motion

From the symmetry considerations, it follows that the motion of test particles in the equatorial plane of the Kerr metric must occur in circular orbits. To see this, one needs to substitute the nonvanishing components of the Christoffel symbols into equation (2.20) and solve it for the circular motion in the equatorial plane $r = r_0$, $\theta = \pi/2$. Thus, we have

$$z^{\mu}(s) = \{t(s), r_0, \pi/2, \Omega_0 t(s)\}, \tag{2.21}$$

where Ω_0 is the orbital frequency of the motion. The four-velocity is given by

$$u^{\mu} = \frac{dz^{\mu}}{ds} = u^0 \{1, 0, 0, \Omega_0\}. \tag{2.22}$$

Indeed, using the Christoffel symbols given in the Appendix for $\beta = 0$, it is easy to show that for the circular motion, the $\mu = 0, 2, 3$ components of equation (2.20) become trivial, whereas the remaining component with $\mu = 1$ has the form

$$\Omega_0^2 \left(1 - a^2 \Omega_s^2\right) - \Omega_s^2 \left(1 - 2a\Omega_0\right) = 0, \tag{2.23}$$

where we have introduced the usual Kepler frequency

$$\Omega_s = \frac{M^{1/2}}{r^{3/2}}. \tag{2.24}$$

From equation (2.23), we find that the orbital frequency of the motion is given by

$$\Omega_0 = \frac{\pm \Omega_s}{1 \pm a\Omega_s}. \tag{2.25}$$

Here and in what follows, the upper sign corresponds to direct orbits (the motion of the particle occurs in the same direction as the rotation of the black hole) and the lower sign refers to retrograde orbits (the particle moves in the opposite direction with respect to the rotation of the black hole). Using this expression in the normalization condition for the four-velocity

$$g_{\mu\nu} u^{\mu} u^{\nu} = -1 = (u^0)^2 \left[1 - a^2 \Omega_0^2 - 3r^2 \Omega_s^2 (1 - a\Omega_0)^2\right], \tag{2.26}$$

16

we obtain the energy of the particle (per unit particle's mass) [19]

$$\frac{E}{m} = \frac{r^2 - 2Mr \pm a\sqrt{Mr}}{r\left(r^2 - 3Mr \pm 2a\sqrt{Mr}\right)^{1/2}},$$
(2.27)

where $E = mu_0$. It follows that when the denominator of this expression vanishes, the energy of the particle becomes infinite, which means that the equation

$$r^2 - 3Mr \pm 2a\sqrt{Mr} = 0$$
(2.28)

determines the radius of the limiting photon orbit. That is, the circular orbits exist in the region $r > r_{ph}$. It is easy to see that in the limiting case $a = M$, we have $r_{ph} = M$ for direct orbits and $r_{ph} = 4M$ for retrograde orbits, while for $a = 0$, $r_{ph} = 3M$.

2.4 Quasi-circular Motion

Let us consider now the motion of test particles in an off-equatorial plane of any stationary axially symmetric metric. In this case, the motion would occur in quasi-circular orbits. In order to describe such orbits, it is convenient to introduce a deviation vector

$$\xi^\mu(s) = x^\mu(s) - z^\mu(s),$$
(2.29)

and expand equation (2.20) in powers of $\xi^\mu(s)$. The resulting equation can be solved using the method of successive approximations. Clearly, at the zeroth-order we have a circular motion in the equatorial plane $\theta = \pi/2$, which is described by $z^\mu(s)$. We note that for the circular motion $u^0 = const$, that allows to pass to the coordinate time t. Taking this into account, we obtain the following equation for the deviation vector [72]

$$\frac{d^2\xi^\mu}{dt^2} + \gamma_\alpha^\mu \frac{d\xi^\alpha}{dt} + \xi^a \partial_a U^\mu = \mathscr{N}^\mu\left(\xi, \frac{d\xi}{dt}\right), \quad a = 1, 2 \equiv r, \theta$$
(2.30)

where $\mathscr{N}^\mu$ stands for all nonlinear terms in $\xi^\mu(s)$ and we have also used the notations

$$\gamma_\alpha^\mu = 2\Gamma_{\alpha\beta}^\mu u^\beta (u^0)^{-1},$$

$$U^\mu = \frac{1}{2}\gamma_\alpha^\mu u^\alpha (u^0)^{-1}.$$
(2.31)

We recall that all coefficients in this equation, including the quantities γ_α^μ and $\partial_a U^\mu$ must be taken on a circular orbit $r = r_0$, $\theta = \pi/2$. At the first-order approximation in $\xi^\mu(s)$, equation (2.30) describes small perturbations around circular orbits. Restricting ourselves to this case and integrating the $\mu = 0, 3$ components of this equation, we obtain

$$\frac{d\xi^A}{dt} + \gamma_r^A \xi^r = 0, \qquad A = 0, 3 \equiv t, \phi. \tag{2.32}$$

Substituting this result in equation (2.30) for $\mu = 1$, we find that it reduces to an equation for harmonic oscillations in the radial direction. Thus, we have

$$\frac{d^2 \xi^r}{dt^2} + \Omega_r^2 \xi^r = 0, \tag{2.33}$$

where the frequency of the radial oscillations is given by

$$\Omega_r = \left(\frac{\partial U^r}{\partial r} - \gamma_A^r \gamma_r^A \right)^{1/2}. \tag{2.34}$$

Similarly, writing down equation (2.30) for $\mu = 2$, we obtain the equation

$$\frac{d^2 \xi^\theta}{dt^2} + \Omega_\theta^2 \xi^\theta = 0, \tag{2.35}$$

which describes harmonic oscillations in the vertical direction with the frequency

$$\Omega_\theta = \left(\frac{\partial U^\theta}{\partial \theta} \right)^{1/2}. \tag{2.36}$$

The above equations in (2.33) - (2.36) can be used to explore the stability of the circular motion against small perturbations. The corresponding stability conditions are given by

$$\Omega_r^2 \geq 0, \qquad \Omega_\theta^2 \geq 0. \tag{2.37}$$

We conclude that *the epicyclic motion of test particles in an arbitrary stationary and axially symmetric spacetime is in essence equivalent (within the linear approximation) to two decoupled oscillations in the radial and vertical directions.*

Turning now to the Kerr metric, we use the Christoffel symbols (A.2) for $\beta = 0$ in the general expression (2.34). After some algebra, we find that the frequency of radial oscillations in the Kerr field is given by [62,70]

$$\Omega_r^2 = \Omega_0^2 \left(1 - \frac{6M}{r} - \frac{3a^2}{r^2} \pm 8a\Omega_s \right). \tag{2.38}$$

From the stability condition in (2.37), it follows that the radius of the innermost stable circular orbit around the Kerr black hole is determined by the equation

$$r^2 - 6Mr - 3a^2 \pm 8a\sqrt{Mr} = 0 \,. \tag{2.39}$$

For a nonrotating black hole, $a = 0$, this equation gives $r = 6M$, while for the limiting rotation case, $a = M$, we find $r = M$ for the direct orbit and $r = 9M$ for the retrograde one.

Similarly, for the frequency of vertical oscillations equation (2.36) gives [62,70]

$$\Omega_\theta^2 = \Omega_0^2 \left(1 + \frac{3a^2}{r^2} \mp 4a\Omega_s \right) \,. \tag{2.40}$$

It is easy to verify that this expression is always nonnegative in the region of existence and the radial stability of the circular motion. That is, the motion is stable with respect to small oscillations in the vertical direction.

Thus, in the Kerr field one can distinguish three fundamental frequencies: The frequency of orbital motion Ω_0 and the frequencies Ω_r and Ω_θ of the epicyclic motion in the radial and vertical directions, respectively. It is important to note that in the Newtonian regime all these frequencies coincide with each other, going over into the usual Kepler frequency ($\Omega_0 = \Omega_r = \Omega_\theta = \Omega_s$). In the Schwarzschild field, $a = 0$, we have only the equality $\Omega_0 = \Omega_\theta = \Omega_s$; the frequency of radial oscillations Ω_r is different. However, in the general case all three frequencies are different from each other, that makes them very attractive for astrophysical implications of the Kerr black holes.

It is also important to estimate the value of these frequencies at radii of physical interest. For this purpose, we first need to define characteristic length and frequency scales in the black hole spacetime. In physical units, we have

$$r_l = \frac{GM}{c^2} \simeq 1.5 \left(\frac{M}{M_\odot} \right) km \,,$$

$$\nu_l = \frac{\Omega_l}{2\pi} = \frac{c^3}{2\pi GM} \simeq 3.2 \cdot 10^4 \left(\frac{M_\odot}{M} \right) Hz \,. \tag{2.41}$$

We recall that here c is the speed of light, G is the gravitational constant and $M_\odot$ is the mass of the Sun. In what follows, we express all other frequencies in terms of the characteristic frequency ν_l. Using expression (2.25) for the orbital

frequency at the ISCO, we find that for $a = 0$

$$v_0 = \frac{\sqrt{6}}{36} v_l \simeq 2.2 \cdot 10^3 \left(\frac{M_\odot}{M} \right) Hz, \quad r = 6M. \tag{2.42}$$

For a maximally rotating black hole, $a = M$, the corresponding maximum orbital frequency for the direct orbit is given by

$$v_0 = \frac{1}{2} v_l \simeq 1.6 \cdot 10^4 \left(\frac{M_\odot}{M} \right) Hz, \quad r = M, \tag{2.43}$$

whereas, for the retrograde orbit, we have

$$v_0 = \frac{1}{26} v_l \simeq 1.2 \cdot 10^3 \left(\frac{M_\odot}{M} \right) Hz, \quad r = 9M. \tag{2.44}$$

A detailed numerical analysis of the orbital and vertical frequencies at ISCOs around a Kerr black hole with mass $M = 10 M_\odot$ is given in Table 2.1 ($v_r = 0$).

Table 2.1: Orbital and vertical frequencies at ISCOs and their ratios.

	direct orbits				retrograde orbits			
a/M	r_{ms}/M	$v_0(Hz)$	$v_\theta(Hz)$	v_0/v_θ	r_{ms}/M	$v_0(Hz)$	$v_\theta(Hz)$	v_0/v_θ
0.00	6.00	217.73	217.73	1.00	6.00	217.73	217.73	1.00
0.10	5.67	235.32	231.91	1.01	6.32	202.54	205.15	0.99
0.20	5.33	255.93	248.03	1.03	6.64	189.28	193.91	0.98
0.30	4.98	280.49	266.52	1.05	6.95	177.59	183.79	0.97
0.40	4.61	310.32	287.97	1.08	7.25	167.20	174.65	0.96
0.50	4.23	347.48	313.16	1.11	7.55	157.92	166.33	0.95
0.60	3.83	395.41	343.20	1.15	7.85	149.56	158.74	0.94
0.70	3.39	460.42	379.58	1.21	8.14	142.02	151.81	0.94
0.80	2.91	556.00	423.99	1.31	8.43	135.12	145.38	0.93
0.90	2.32	721.41	474.68	1.52	8.72	128.84	139.47	0.92
0.99	1.24	1348.05	304.86	4.42	8.99	123.19	134.10	0.92

We note that as the rotation parameter of the black hole grows, the radius of the direct ISCO moves towards the event horizon and the associated orbital frequency increases, approaching its maximum value in (2.43) at the horizon. The vertical epicyclic frequency increases to its maximum value and then decreases to zero ($v_\theta = 0$ for $a = M$, $r = M$). The ratio of these frequencies v_0/v_θ essentially differs from unity only for the fast enough rotation of the black hole. For the retrograde motion both the frequencies decrease with the growth of the rotation parameter, whereas their ratio remains about unity.

It is also of interest to calculate all three frequencies at direct stable orbits with radii $r > r_{ISCO}$ around a maximally rotating black hole, $a = M$. The results of numerical calculations are given in Table 2.2.

Table 2.2: Frequencies at radii $r > r_{ISCO}$.

r/M	ν_r(Hz)	ν_θ(Hz)	ν_0(Hz)	ν_θ/ν_r	ν_0/ν_r	ν_0/ν_θ
2.00	234.08	484.35	835.85	2.07	3.57	1.73
2.30	244.60	462.27	712.99	1.89	2.91	1.54
2.90	237.48	398.45	538.85	1.68	2.27	1.35
3.50	217.25	337.58	423.96	1.55	1.95	1.26
3.80	206.12	311.02	380.61	1.51	1.85	1.22
4.10	195.14	287.13	344.02	1.47	1.76	1.20
4.30	**188.05**	**272.60**	**322.69**	**1.45**	**1.72**	**1.18**
4.60	177.86	252.71	294.50	1.42	1.66	1.17
4.90	168.28	234.89	270.12	1.40	1.61	1.15
5.00	**165.23**	**229.37**	**262.72**	**1.39**	**1.59**	**1.15**
5.30	156.49	213.94	242.40	1.37	1.55	1.13
5.60	148.36	200.05	224.53	1.35	1.51	1.12
5.90	140.81	187.51	208.73	1.33	1.48	1.11
6.20	133.80	176.17	194.67	1.32	1.45	1.11
6.50	127.30	165.87	182.11	1.30	1.43	1.10
6.80	121.27	156.50	170.83	1.29	1.41	1.09
7.00	**117.48**	**150.71**	**163.93**	**1.28**	**1.40**	**1.09**

It is worth noting that at some particular orbits near the black hole, the predicted values of these frequencies (bolded in the table) are in good qualitative agreement with the corresponding frequencies of twin peaks QPOs, which have been detected in some black hole binaries: For instance, with **(184, 276 Hz)** for X-ray binary XTE J1550-564; with **(165, 241 Hz)** for X-ray binary H1743-322; with **(113, 168 Hz)** for X-ray binary GRS 1915 + 105.

2.5 The Highest Epicyclic Frequencies

It is curious that there exists *the highest frequency* for small radial oscillations around circular orbits in the Kerr field. Evaluating the first derivative of the expression in (2.38) with respect to r, we obtain the equation

$$r^3 (8M - r) + a^2 \left(5r^2 - 4Mr\right) \pm 2a\sqrt{Mr} \left[a^2 + r (M - 6r)\right] = 0 . \tag{2.45}$$

This equation determines the radii for both direct and retrograde orbits, at which the radial epicyclic frequency attains its highest value. For $a = 0$, it follows that

$r_{max} = 8M$. The associated frequency is

$$\nu_{r(max)} \simeq 707.1 \left(\frac{M_\odot}{M} \right) Hz. \tag{2.46}$$

In the general case, one can solve equation (2.45) only numerically. In particular, for $a = M$ and for direct orbits, we find that $r_{max} \simeq 2.4M$ and

$$\nu_{r(max)} \simeq 2453 \left(\frac{M_\odot}{M} \right) Hz. \tag{2.47}$$

Similarly, for retrograde orbits at $a = M$, we have $r_{max} \simeq 11.8M$ and

$$\nu_{r(max)} \simeq 422.6 \left(\frac{M_\odot}{M} \right) Hz. \tag{2.48}$$

In Figure 2.1 we plot the dependence of the radial epicyclic frequency on the radii of circular orbits around a Kerr black hole for different values of the rotation parameter and for $M = 10M_\odot$.
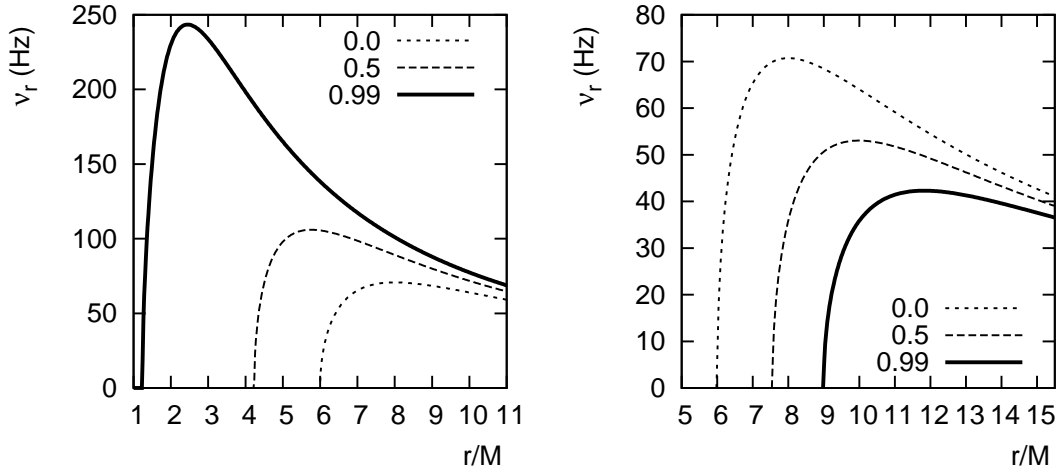

Figure 2.1: Radial epicyclic frequencies with three values of the rotation parameter $a = 0$, 0.5 and 0.99. *Left*: For direct orbits. *Right*: For retrograde orbits.

The full numerical analysis of equation (2.45) and the associated values of the radial, vertical and orbital frequencies along with their corresponding ratios are presented in Tables 2.3 and 2.4.

We note that with increasing rotation parameter of the black hole, the maxima of the radial epicyclic frequency shifts towards the event horizon and in the limiting case $a = M$, the frequency attains its highest value in the near-horizon region. The accompanying vertical and orbital frequencies at the same radii also increase to their highest values for $a = M$. It is also interesting to note that the characteristic ratios $\nu_\theta : \nu_{r(max)} = 2 : 1$, $\nu_0 : \nu_{r(max)} = 2 : 1$ and $\nu_0 : \nu_\theta = 1 : 1$

22

Table 2.3: The highest radial frequency and the associated vertical and orbital frequencies at direct orbits ($M = 10M_\odot$).

a/M	r_{max}/M	ν_r(Hz)	ν_θ(Hz)	ν_0(Hz)	ν_θ/ν_r	ν_0/ν_r	ν_0/ν_θ
0.00	8.00	70.71	141.42	141.42	2.00	2.00	1.00
0.10	7.58	75.73	151.17	152.60	2.00	2.02	1.01
0.20	7.15	81.52	162.37	165.68	1.99	2.03	1.02
0.30	6.70	88.27	175.45	181.26	1.99	2.05	1.03
0.40	6.24	96.29	190.74	199.97	1.98	2.08	1.05
0.50	5.76	105.99	209.23	223.29	1.97	2.11	1.07
0.60	5.26	118.03	231.78	252.90	1.96	2.14	1.09
0.70	4.71	133.53	260.59	292.71	1.95	2.19	1.12
0.80	4.11	154.57	298.90	349.83	1.93	2.26	1.17
0.90	3.42	185.95	353.95	442.93	1.90	2.38	1.25
0.99	2.45	243.45	447.52	662.11	1.84	2.72	1.48
1.00	2.42	245.34	450.40	671.62	1.84	2.74	1.49

remain almost unchanged up to large enough values of the rotation parameter. However, for $a \to M$ we have approximate ratios $\nu_\theta : \nu_r = 9 : 5$, $\nu_0 : \nu_r = 5 : 2$ and $\nu_0 : \nu_\theta = 3 : 2$. *Thus, we conclude that at characteristic stable circular orbits, where the radial epicyclic frequency attains its highest value, the ratio $\nu_\theta : \nu_r = 2 : 1$ remains nearly the same even for $a \to M$.* Remarkably, this fact is in good agreement with the observed twin QPOs frequencies in the X-ray spectrum of some black hole binaries. For instance, for $a \simeq (0.8$–$0.9)M$, the detected pair **(164, 328 Hz)** in the source GRS 1915 + 105 falls in the expected ranges of the radial ν_r and vertical ν_θ epicyclic frequencies given in Table 2.3.

Table 2.4: The highest radial frequency and the associated vertical and orbital frequencies at retrograde orbits ($M = 10M_\odot$).

a/M	r_{max}/M	ν_r(Hz)	ν_θ(Hz)	ν_0(Hz)	ν_θ/ν_r	ν_0/ν_r	ν_0/ν_θ
0.00	8.00	70.71	141.42	141.42	2.00	2.00	1.00
0.10	8.41	66.31	132.83	131.72	2.00	1.99	0.99
0.20	8.81	62.42	125.20	123.24	2.01	1.97	0.98
0.30	9.21	58.95	118.38	115.74	2.01	1.96	0.98
0.40	9.60	55.84	112.25	109.08	2.01	1.95	0.97
0.50	9.98	53.03	106.70	103.10	2.01	1.94	0.97
0.60	10.36	50.48	101.65	97.72	2.01	1.94	0.96
0.70	10.73	48.16	97.04	92.85	2.02	1.93	0.96
0.80	11.10	46.03	92.81	88.41	2.02	1.92	0.95
0.90	11.47	44.07	88.92	84.35	2.02	1.91	0.95
1.00	11.83	42.26	85.32	80.63	2.02	1.91	0.95

From this table we see that the highest value of the radial frequency for $a = 0$ as well as the associated values of the vertical and orbital frequencies decrease with the growth of the rotation parameter and attain their characteristic values in the limiting case $a = M$. It is curious that in all cases the frequencies exhibit, to a good enough accuracy, the ratios $\nu_\theta : \nu_{r(max)} = 2 : 1$, $\nu_0 : \nu_{r(max)} = 2 : 1$ and $\nu_0 : \nu_\theta = 1 : 1$.

Let us now consider the expression for the vertical epicyclic frequency given in (2.40). It turns out that for direct orbits and for sufficiently large values of the rotation parameter this frequency also attains its highest value. Similar to the case of the radial frequency described above, one can show that the radii of characteristic direct orbits, pertaining to the maxima of the vertical frequency, obey the equation

$$r\left[r^3 + a^2\left(5r - 2M\right)\right] + 2a\sqrt{Mr}\left(a^2 - 3r^2\right) = 0 . \tag{2.49}$$

Solving this equation numerically for $a = M$, we find that $r \simeq 1.86$ and the vertical frequency has the highest value

$$\nu_{\theta(max)} \simeq 4875\left(\frac{M_\odot}{M}\right)Hz . \tag{2.50}$$

The radial frequency at this radius has the value

$$\nu_r \simeq 2236\left(\frac{M_\odot}{M}\right)Hz . \tag{2.51}$$

It is worth noting that an approximate ratio $\nu_{\theta(max)} : \nu_r = 2 : 1$ holds in this case as well.

In Figure 2.2 we plot the vertical epicyclic frequency as a function of the radius of direct orbits, for given values of the rotation parameter and for $M = 10M_\odot$ (*Left*), and the positions of ISCOs and $\nu_{\theta(max)}$ as functions of the rotation parameter (*Right*). We see that in the region of physical interest, $r > r_{ISCO}$, the vertical frequency reaches its highest value.
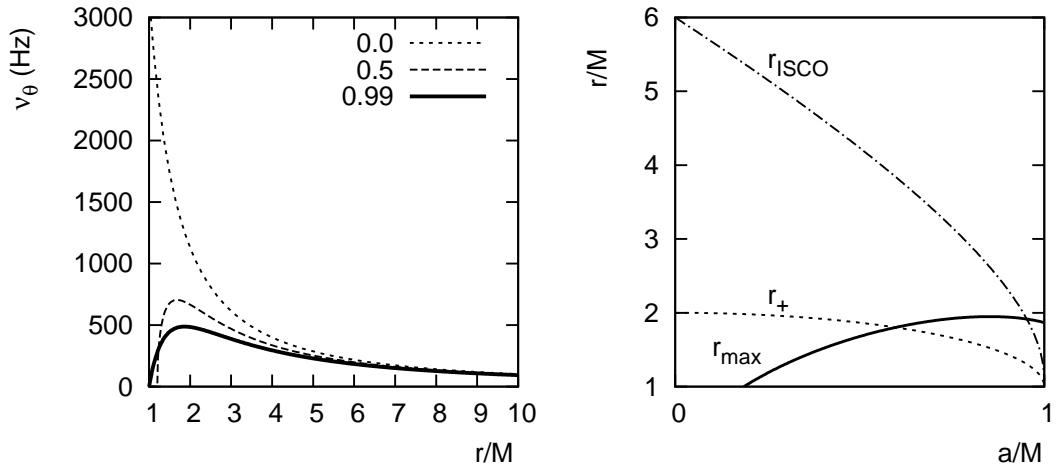
Figure 2.2: *Left*: Vertical epicyclic frequencies with $a = 0, 0.5$ and 0.99. *Right*: Positions of ISCO and $\nu_{\theta(max)}$ as functions of a.

3. ROTATING BRANEWORLD BLACK HOLES

As we have described in Chapter 1, an intriguing approach to the problem of finding an exact solution for a rotating black hole localized on the Randall-Sundrum 3-brane was undertaken in [39]. The authors postulated that the induced metric on the 3-brane embedded into a five-dimensional bulk space can be taken as a stationary and axisymmetric Kerr-Schild type metric. Solving the effective gravitational equations on the brane with this metric ansatz, they presented a Kerr-Newman type solution, which carries the signature of the fifth dimension through a Coulomb type tidal charge. The appearance of this charge is the result of gravitational interaction between the brane and the bulk, that is transmitted on the brane by the "electric" part of the bulk Weyl tensor.

The effective gravitational field equations on a 3-brane in the Randall and Sundrum scenario were first derived in [27], using the Gauss-Codazzi projective approach and the Gaussian normal coordinates. Later on, these equations were also obtained in a more general Arnowitt, Deser and Misner (ADM) type approach, which allows for acceleration of the normals to the brane surface, introducing the lapse shift functions [28]. In the most simple case, when the bulk space is empty, these equations have the form

$$R_{ij} = -E_{ij}, \qquad i = 0, 1, 2, 3, \tag{3.1}$$

where E_{ij} is the traceless "electric part" of the five-dimensional Weyl tensor

$$E_{ij} = {}^{(5)}C_{ABCD} \, n^A \, n^C e_i^B e_j^D, \qquad A = 0, 1, 2, 3, 4, \tag{3.2}$$

and the associated Hamiltonian constraint equation is given by

$$R = 0. \tag{3.3}$$

We recall that in the Randall-Sundrum braneworld scenario the momentum constraint equation becomes trivial. Furthermore, the cosmological constant on the brane vanishes due to the fine-tuning condition (see for details [39]).

3.1 The Metric and Its Properties

The exact solution to the effective gravitational field equations on the 3-brane given by (3.1) and (3.3) that describes rotating black holes is given by the metric [39]

$$ds^2 = -\frac{\Delta}{\Sigma}\left(dt - a\sin^2\theta\, d\phi\right)^2 + \Sigma\left(\frac{dr^2}{\Delta} + d\theta^2\right) + \frac{\sin^2\theta}{\Sigma}\left[adt - (r^2 + a^2)\,d\phi\right]^2, \quad \textbf{(3.4)}$$

where the metric functions

$$\Delta = r^2 + a^2 - 2Mr + \beta \quad,$$

$$\Sigma = r^2 + a^2\cos^2\theta \tag{3.5}$$

and M is the mass, a is the rotation parameter or the angular momentum per unit mass $(a = J/M)$ and β is the tidal charge.

It should be noted that the field equations (3.1) are not closed on the brane as they involve the quantities E_{ij} of the higher-dimensional origin. Therefore, the metric (3.4) exactly solves the constraint equation (3.3) and when substituting in equation (3.1) it closes the system by specifying the "source" E_{ij} on the right-hand side. Having performed explicit calculations, we find [39]

$$E_t{}^t = -E_\phi{}^\phi = -\frac{\beta}{\Sigma^3}\left[\Sigma - 2\left(r^2 + a^2\right)\right],$$

$$E_r{}^r = -E_\theta{}^\theta = \frac{\beta}{\Sigma^2}, \tag{3.6}$$

$$E_\phi{}^t = -(r^2 + a^2)\sin^2\theta\, E_t{}^\phi = -\frac{2\beta a}{\Sigma^3}\left(r^2 + a^2\right)\sin^2\theta.$$

With these quantities, it is straightforward to show that the conservation law $D_i E_j^i = 0$ is identically satisfied on the brane. Comparing the asymptotic behavior of these quantities with that of the energy-momentum tensor for the usual

Kerr-Newman black hole in general relativity

$$T_t{}^t = -T_\phi{}^\phi = \frac{Q^2}{8\pi\Sigma^3}\left[\Sigma - 2\left(r^2 + a^2\right)\right] ,$$

$$T_r{}^r = -T_\theta{}^\theta = -\frac{Q^2}{8\pi\Sigma^2} , \tag{3.7}$$

$$T_\phi{}^t = -\left(r^2 + a^2\right)\sin^2\theta\, T_t{}^\phi = \frac{Q^2 a}{4\pi\Sigma^3}\left(r^2 + a^2\right)\sin^2\theta ,$$

we conclude that the parameter β in the metric (3.4) must create Coulomb-type effects just as the square of the electric charge in the Kerr-Newman solution. That is, though we have no electric charge on the brane, the rotating black hole solution on the brane turns out to be inevitably "charged" due to the tidal influence of the bulk space. It is important to note that, unlike the case of the Kerr-Newman solution, the tidal charge in (3.4) may have both *positive* and *negative* values. For $a = 0$, the metric (3.4) reduces to a Reissner-Nordstrom type solution with a tidal charge, which describes a static braneworld black hole [38]. For $\beta = 0$, we have the usual Kerr solution in general relativity [16]. The physical properties of the metric (3.4) are largely similar to those of the Kerr-Newman metric in general relativity. However, some significant differences do exist as well.

The event horizon structure of the metric (3.4) is determined by the equation $\Delta = 0$, or equivalently by

$$\Delta = r^2 + a^2 - 2Mr + \beta = 0. \tag{3.8}$$

The largest root of this equation

$$r_+ = M + \sqrt{M^2 - a^2 - \beta} \tag{3.9}$$

corresponds to the radius of the horizon. It is important to note that the event horizon, as it follows from equation (3.9), exists provided that

$$M^2 \geq a^2 + \beta , \tag{3.10}$$

where the equality corresponds to a maximally rotating black hole. As in the case of the Kerr metric, this is dictated by a Cosmic Censor. We note that when the tidal charge is positive, the condition in (3.10) gives rise to the Kerr type bound on the angular momentum: *the rotating braneworld black hole with a positive tidal charge must possess an angular momentum not exceeding its mass.*

However, the situation is significantly different for a negative tidal charge. In fact, for a rotating black hole with $\beta < 0$ and $a = M$, equation (3.9) gives

$$r_+ = \left(M + \sqrt{-\beta}\right) > M. \tag{3.11}$$

That is, for the maximally rotating black hole with the horizon radius $r_+ = M$ the angular momentum is greater than the mass. Thus, *braneworld gravity admits a rotating black hole, whose angular momentum may exceed its mass*. This fairly breaches the Kerr bound in general relativity.

Another important feature of the rotating braneworld black hole is related to the norm of the timelike Killing vector $\xi_{(t)}$, which does not vanish on the horizon. From the equation

$$\xi_{(t)} \cdot \xi_{(t)} = g_{tt} = 0, \tag{3.12}$$

we find that

$$r_0 = M + \sqrt{M^2 - a^2 \cos^2 \theta - \beta}, \tag{3.13}$$

where r_0 is the largest root of this equation and describes the boundary of the ergosphere around the braneworld black hole. It is easy to see from equation (3.13) that the negative tidal charge extends the ergosphere around the braneworld black hole, whereas the positive tidal charge decreases it [39]. In the limiting case, substituting equation (3.10) in (3.13), we find that the radius of the ergosphere falls in the range

$$M < r < M + \sin \theta \sqrt{M^2 - \beta}. \tag{3.14}$$

It follows that rotating braneworld black holes with negative tidal charge must be more energetic objects compared to those with positive tidal charge.

3.2 Circular Motion

As in the case of the Kerr metric, the circular motion of test particles occurs in the equatorial plane of the metric (3.4). Substituting the nonvanishing components of the Christoffel symbols (A.2) in equation (2.20), we follow the steps, leading

to equations (2.21)-(2.25) of Chapter 2. Consequently, we find that the Kepler frequency is given by

$$\Omega_s = \frac{(Mr - \beta)^{1/2}}{r^2},$$ (3.15)

whereas for the orbital frequency of the motion we obtain

$$\Omega_0 = \frac{\pm \Omega_s}{1 \pm a\Omega_s}.$$ (3.16)

Again, using the normalization condition for the four-velocity

$$g_{\mu\nu}u^\mu u^\nu = -1 = (u^0)^2 \left[1 - a^2\Omega_0^2 - 3r^2\Omega_s^2(1 - a\Omega_0)^2\right],$$ (3.17)

we find the energy of the particle (per unit particle's mass)

$$\frac{E}{m} = \frac{r^2 - 2Mr + \beta \pm a\sqrt{Mr - \beta}}{r\left[r^2 - 3Mr + 2\beta \pm 2a\sqrt{Mr - \beta}\right]^{1/2}}.$$ (3.18)

For $\beta = 0$, this expression coincides with that given in (2.27). It follows that the radius of the limiting photon orbit is determined by the equation

$$r^2 - 3Mr + 2\beta \pm 2a\sqrt{Mr - \beta} = 0.$$ (3.19)

In the general case, when $\beta \neq 0$ equation (3.19) can be solved only numerically. In particular, one can verify that for $a = 0$ and $\beta = -M^2$, the radius of the photon orbit $r_{ph} \simeq 3.56M$, whereas the radius of the event horizon $r_+ = (1 + \sqrt{2})M$. For the positive tidal charge $\beta = M^2$, we have the same limiting radii as for the Reissner-Nördstrom metric. That is, $r_{ph} = 2M$ and $r_+ = M$. We recall that for a rotating braneworld black hole with a negative tidal charge, the rotation parameter $a > M$. For instance, for $\beta = -M^2$, we have the limiting value $a = \sqrt{2}M$. In this case, $r_+ = M$ and $r_{ph} = M$ in the direct motion, whereas $r_{ph} = 4.82M$ in the retrograde motion. Further details can be found in [39].

3.3 Epicyclic Frequencies

The explicit expressions for the radial and vertical epicyclic frequencies in the field of the rotating braneworld black holes can be obtained by substituting the Christoffel symbols (A.2) into the general expressions (2.34) and (2.36). Having

performed all calculations, we find that the frequency of radial oscillations is given
by

$$\Omega_r^2 = \frac{\Omega_0^2}{Mr - \beta} \left[Mr \left(1 - \frac{6M}{r} - \frac{3a^2}{r^2} + \frac{9\beta}{r^2} \right) + \frac{4\beta}{r^2}(a^2 - \beta) \pm 8a\Omega_s(Mr - \beta) \right], \quad \textbf{(3.20)}$$

where Ω_0 is the same as that given in (3.16). Similarly, for the frequency of
vertical oscillations we obtain

$$\Omega_\theta^2 = \Omega_0^2 \left[1 + \frac{a^2}{r^2} \left(1 + \frac{2Mr - \beta}{Mr - \beta} \right) \mp 2a\Omega_s \frac{2Mr - \beta}{Mr - \beta} \right]. \quad \textbf{(3.21)}$$

We note that these expressions agree with the uncharged test particle limit of the
general formulas given in [62] for the Kerr-Newman metric.

The vanishing of the radial epicyclic frequency in (3.20) determines the radius of
the innermost stable circular orbit, for which we have the equation

$$Mr \left(1 - \frac{6M}{r} - \frac{3a^2}{r^2} + \frac{9\beta}{r^2} \right) + \frac{4\beta}{r^2}(a^2 - \beta) \pm 8a\Omega_s(Mr - \beta) = 0. \quad \textbf{(3.22)}$$

Solving this equation numerically, we find that for $a = 0$ and $\beta = -M^2$, the
radius of the ISCO tends to $r_{ms} \simeq 7.3M$ and $r_+ = (1 + \sqrt{2})M$, whereas for
$\beta = M^2$, $r_{ms} = 4M$ and $r_+ = M$. In the latter case, the radii are the same as
those for an extreme Reissner-Nördstrom black hole. On the other hand, for a
maximally rotating black hole with the negative charge $\beta = -M^2$ and $a = \sqrt{2}M$,
we obtain that $r_{ms} = M$ for the direct ISCO and $r_{ms} \simeq 11.25M$ for the retrograde
ISCO. We recall that $r_+ = M$. The full numerical analysis show that the negative
tidal charge has an expelling effect on both direct and retrograde orbits, while
the positive tidal charge appears to have the opposite effect [39].

A similar numerical analysis of the expression (3.21) shows that it is nonnegative
in the physical region. That is, the circular motion around the braneworld black
hole is always stable to linear perturbations in the vertical direction.

It turns out that, just as in the Kerr field, the radial epicyclic frequency in (3.20)
has a maxima at some characteristic radii. In what follows, we focus on this
case. Assuming that the black hole has a small positive tidal charge, we compute
all three frequencies and their corresponding ratios at radii, for which the radial
frequency attains its maximum value. The numerical results are summarized in
Table 3.1.

Table 3.1: The highest radial frequency and the associated vertical and orbital frequencies for the positive tidal charge.

	Direct orbits: $\beta = 0.1M^2$, $M = 10M_\odot$						
a/M	r_{max}/M	ν_r(Hz)	ν_θ(Hz)	ν_0(Hz)	ν_θ/ν_r	ν_0/ν_r	ν_0/ν_θ
0.00	7.81	72.78	145.69	145.69	2.00	2.00	1.00
0.09	7.41	77.83	155.54	156.99	2.00	2.02	1.01
0.19	6.99	83.65	166.83	170.17	1.99	2.03	1.02
0.28	6.56	90.42	179.91	185.77	1.99	2.05	1.03
0.38	6.12	98.43	195.30	204.58	1.98	2.08	1.05
0.47	5.66	108.10	213.71	227.80	1.98	2.11	1.07
0.57	5.17	120.05	236.29	257.38	1.97	2.14	1.09
0.66	4.64	135.38	264.85	296.79	1.96	2.19	1.12
0.76	4.07	156.08	302.77	353.12	1.94	2.26	1.17
0.85	3.39	186.74	357.31	444.84	1.91	2.38	1.24
0.95	2.42	244.13	452.24	666.79	1.85	2.73	1.47

Comparing these results with those given in Table 2.3, we see that the observed pair of frequencies **(164, 328 Hz)** in the source GRS 1915 + 105 falls in the range of the radial ν_r and vertical ν_θ frequencies, corresponding to less values of the rotation parameter, $a \simeq (0.7\text{--}0.8)M$. Meanwhile, recent observations give the lower bound $a > 0.98M$ on the rotation parameter of the black hole in GRS 1915 + 105 [77]. In this sense, one can conclude that *the positive tidal charge is not supported by observations of black holes*.

Next, we suppose that the black hole possesses the negative tidal charge $\beta = -M^2$ and calculate all three frequencies at characteristic direct orbits, at which the radial epicyclic frequency attains its maxima. The results are given in Table 3.2.

Again, comparing these results with those given in Table 2.3, we see that the negative tidal charge increases the radii r_{max}, whereas with increasing the rotation parameter of the black hole, the radii again move towards the event horizon, approaching the limiting value for $a = \sqrt{2}M$. It is important to note that in the over-rotating case, $a \simeq 1.27M$, the values of the radial ν_r and vertical ν_θ frequencies and their ratio are in good agreement with the detected pair of frequencies **(164, 328 Hz)** in the source GRS 1915 + 105.

Figure 3.1 displays the positions of maxima of the radial epicyclic frequencies for an extreme Kerr black hole and for a maximally rotating black hole with the

Table 3.2: The highest radial frequency and the associated vertical and orbital frequencies for the negative tidal charge.

a/M	r_{max}/M	ν_r(Hz)	ν_θ(Hz)	ν_0(Hz)	ν_θ/ν_r	ν_0/ν_r	ν_0/ν_θ
Direct orbits: $\beta = -M^2$, $M = 10M_\odot$							
0.00	9.64	56.20	112.29	112.29	2.00	2.00	1.00
0.14	9.09	60.69	121.06	122.28	1.99	2.01	1.01
0.28	8.53	65.94	131.25	134.11	1.99	2.03	1.02
0.42	7.95	72.15	143.25	148.35	1.99	2.06	1.04
0.57	7.36	79.63	157.61	165.82	1.98	2.08	1.05
0.71	6.74	88.84	175.16	187.83	1.97	2.11	1.07
0.85	6.09	100.51	197.15	216.53	1.96	2.15	1.10
0.99	5.40	115.87	225.74	255.80	1.95	2.21	1.13
1.13	4.64	137.33	264.91	313.73	1.93	2.28	1.18
1.27	3.77	170.50	323.56	411.81	1.90	2.42	1.27
1.41	2.53	236.74	431.78	663.00	1.82	2.80	1.54

tidal charge $\beta = -M^2$. We see that the epicyclic frequencies in the field of these black holes are observationally almost indistinguishable. Thus, *unlike the case of positive tidal charge, the existence of the negative tidal charge could be in agreement with observations of black holes.* Clearly, in this case the angular momentum of the black hole has a crucial meaning. It may happen that the precise measurements of the angular momentum with future independent observational data gives results, that breaches the Kerr bound $a = M$. Then our results with the negative tidal charge would have a great significance for describing the signature of the extra dimension in the real universe.
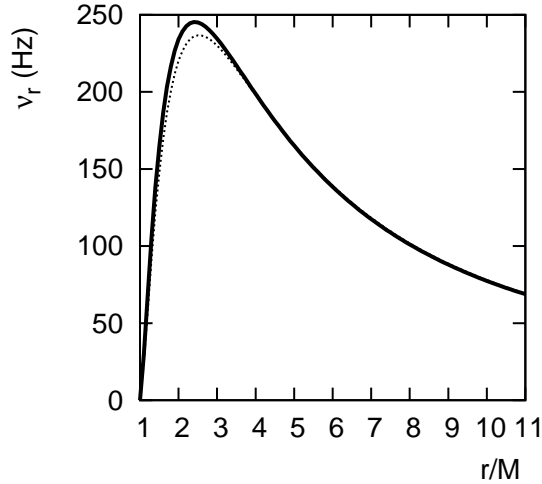

Figure 3.1: The radial epicyclic frequencies. The solid line corresponds to $\beta = 0$, $a = M$ and the dotted line refers to $\beta = -M^2$, $a = \sqrt{2}M$.

3.4 Relativistic Precessions

As we have seen above, orbits of test particles around rotating black holes with or without tidal charge can be described in terms of three fundamental frequencies. The fact that these frequencies are all different from each other results in two familiar relativistic precession effects: (i) The effect of periastron precession, which in the weak-field regime describes the precession of the semi-major axis of elliptic orbits, (ii) Frame-dragging effect, which in the weak field limit corresponds to the Lense-Thirring precession around a rotating body [15]. It is interesting to ask the following question: *Whether the frequencies of these precessions could have a viable meaning in the context of high-frequency QPOs seen in some black hole binaries*? Below, we try to answer this question.

The difference between the orbital frequency and the radial epicyclic frequency causes the periastron precession. This leads to a secular shift in the perihelion of an elliptic orbit. Following the work of [71], we define the associated angular displacement per one revolution as

$$\Delta\phi = 2\pi \left| 1 - \frac{\Omega_0}{\Omega_r} \right|. \tag{3.23}$$

Consequently, for the coordinate frequency of the periastron precession we obtain

$$\Omega_{PP} = \left| \Omega_0 - \Omega_r \right|. \tag{3.24}$$

Similarly, the non-coincidence of the vertical epicyclic frequency with the orbital frequency of the motion causes dragging of the orbital plane in the direction of rotation. This gravitomagnetic phenomenon is the reason for the precession of the orbital plane around the axis of symmetry. The precession angle per one revolution is given by [71]

$$\Delta\phi = 2\pi \left| 1 - \frac{\Omega_0}{\Omega_\theta} \right|. \tag{3.25}$$

And the corresponding precession frequency is

$$\Omega_{LT} = \left| \Omega_0 - \Omega_\theta \right|. \tag{3.26}$$

We recall that as $\Omega_0 > \Omega_\theta > \Omega_r$, both precession effects refer to direct orbits. With the radial and vertical epicyclic frequencies given in (3.20) and (3.21), it is

easy to show that for maximally rotating black holes both precession frequencies Ω_{PP} and Ω_{LT} on the horizon reduce to the angular velocity of the horizon.

Next, focusing at characteristic radii, at which the radial epicyclic frequency reaches its maximum value, we have computed the precession frequencies and their ratio. For zero tidal charge the results are summarized in Table 3.3.

Table 3.3: Relativistic precession frequencies.

Direct orbits: $\beta = 0$, $M = 10M_\odot$				
a/M	r_{max}/M	ν_{PP}(Hz)	ν_{LT}(Hz)	ν_{LT}/ν_{PP}
0.00	8.00	70.71	0.00	0.00
0.10	7.58	76.89	1.43	0.02
0.20	7.15	84.19	3.31	0.04
0.30	6.70	92.96	5.81	0.06
0.40	6.24	103.71	9.24	0.09
0.50	5.76	117.26	14.06	0.12
0.60	5.26	134.92	21.13	0.16
0.70	4.71	159.16	32.12	0.20
0.80	4.12	195.16	50.90	0.26
0.90	3.42	257.23	89.09	0.35
1.00	2.42	426.28	221.21	0.52

We note that the ratio of these frequencies gradually increases and for high enough values of the rotation parameter, the integer ratios $\nu_{PP} : \nu_{LT} = 3 : 1$ and $\nu_{PP} : \nu_{LT} = 2 : 1$ appear. Furthermore, the value of these frequencies fall in the expected ranges of high-frequency QPOs in black hole binaries.

We have also computed these frequencies for the negative tidal charge $\beta = -M^2$. Comparing the results with those given in Table 3.3, we have plotted both cases in Figure 3.2.

This figure clearly shows that for maximally rotating black holes, when the rotation parameter is either $a = M$ or $a = \sqrt{2}M$, the corresponding precession frequencies in the field of the black holes with zero tidal charge and with the tidal charge $\beta = -M^2$ become observationally indistinguishable. It is also worth noting that in both cases the limiting ratio tends to $\nu_{PP} : \nu_{LT} = 2 : 1$. We conclude that *for sufficiently fast rotation of the black holes, the relativistic precession frequencies at characteristic radii fall in the expected ranges of high-frequency QPOs in black hole binaries. Furthermore, the model admits the special frequency*
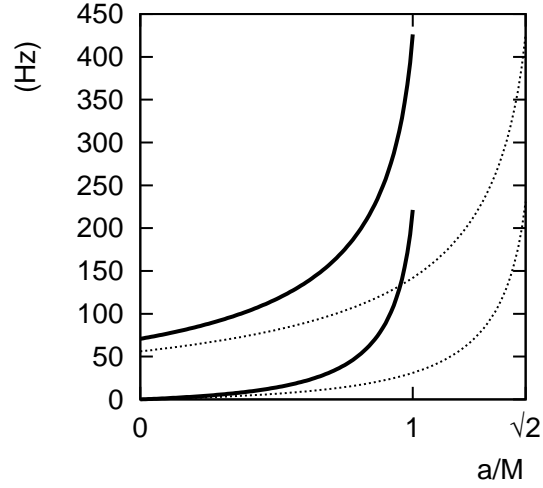
Figure 3.2: Relativistic precession frequencies as functions of the rotation parameter. The upper solid curve corresponds to ν_{PP} and the lower solid line refers to ν_{LT}. Similarly, the dotted curves correspond to the case with nonzero tidal charge.

ratios: $\nu_{PP} : \nu_{LT} = 3 : 1$ *and* $\nu_{PP} : \nu_{LT} = 2 : 1$. Again, the precise measurements of the angular momentum from independent observations (for instance, from relativistically-broadened Fe Kα line formed near the ISCO) would have to play a crucial role in identification of the observed black holes with their real prototypes. Thus, a measured value of the rotation parameter, obeying the inequality $a > M$ would signal in favor of the higher-dimensional nature of the black holes.

4. CONCLUSION

Below, we briefly formulate the basic results of this thesis.

1. We have given an overview of the current theoretical status of black holes in general relativity and braneworld gravity. We have also given an overview of modern observations of black holes in X-ray binaries, describing unusual properties of the X-ray sources, such as the appearance of high-frequency quasi-periodic oscillations in the X-ray spectra.

2. In the framework of the theory of epicyclic motion of test particles in stationary and axisymmetric spacetimes, developed earlier by Aliev and Gal'tsov, we have rederived the expressions for the orbital, radial and vertical epicyclic frequencies in the Kerr field.

3. We have performed the full numerical analysis of these frequencies at both innermost stable circular orbits and beyond them. We have found that the values of the radial and vertical epicyclic frequencies at some particular orbits are in good qualitative agreement with the frequencies of twin peaks quasi-periodic oscillations that have been detected in some black hole binaries.

4. We have considered the model of particle's motion, for which the radial (or vertical) epicyclic frequency at some characteristic radii attains its highest value. We have shown that in this model the epicyclic frequencies exhibit the ratio $\nu_\theta : \nu_{r(max)} = 2 : 1$ (or $\nu_{\theta(max)} : \nu_r = 2 : 1$), which remains nearly the same even for a maximally rotating Kerr black hole, $a \to M$.

5. We have studied the motion of test particles in the field of a rotating black hole in the Randall-Sundrum braneworld scenario. This black hole possesses a tidal charge that transmits into our observable world the signature of an extra spacelike dimension. We have presented analytical expressions for the frequencies of oscillations in the radial and vertical directions. Considering a particular model, in which the radial epicyclic frequency reaches its maximum value, we

have given a detailed numerical analysis of these frequencies. We have shown that the existence of the negative tidal charge could be in agreement with modern observations of black holes.

6. We have explored relativistic precession effects, periastron and frame-dragging, in the field of rotating Kerr and braneworld black holes. We have shown that for sufficiently fast rotation of these black holes, the relativistic precession frequencies at characteristic radii fall in the expected ranges of high-frequency QPOs in black hole binaries. Moreover, they exhibit $3:1$ and $2:1$ ratios.

REFERENCES

[1] **Maldacena, J.M.**, 1998. The Large N Limit of Superconformal Field Theories and Supergravity, *Adv. Theor. Math. Phys.*, **2**, 231–252.

[2] **Gubser, S.S.**, **Klebanov, I.R. and Polyakov, A.M.**, 1998. Gauge Theory Correlators from Non-Critical String Theory, *Phys.Lett. B*, **428**, 105–114.

[3] **Witten, E.**, 1998. Anti De Sitter Space And Holography, *Adv. Theor. Math. Phys.*, **2**, 253–291.

[4] **Aharony, O.**, **Gubser, S.S.**, **Maldacena, J.M.**, **Ooguri, H. and Oz, Y.**, 2000. Large N Field Theories, String Theory and Gravity, *Phys. Rept.*, **323**, 183–386.

[5] **Hawking, S.W.**, **Hunter, C.J. and Taylor-Robinson, M.M.**, 1999. Rotation and the AdS/CFT correspondence, *Phys. Rev. D*, **59**, 064005.

[6] **Penrose, R.**, 1965. Gravitational Collapse and Space-time Singularities, *Phys. Rev. Lett.*, **14**, 57–59.

[7] **Hawking, S.W. and Penrose, R.**, 1970. The Singularities of gravitational collapse and cosmology, *Proc. Roy. Soc. Lond.*, **A314**, 529–548.

[8] **Israel, W.**, 1967. Event Horizons in Static Vacuum Space-times, *Phys. Rev.*, **164**, 1776–1779.

[9] **Carter, B.**, 1971. Axisymmetric Black Hole Has Only Two Degrees of Freedom, *Phys. Rev. Lett.*, **26**, 331–333.

[10] **Hawking, S.W.**, 1972. Black Holes in General Relativity, *Commun. Math. Phys.*, **25**, 152–166.

[11] **Robinson, D.C.**, 1975. Uniqueness of the Kerr Black Hole, *Phys.Rev.Lett.*, **34**, 905–906.

[12] **Carter, B.**, 1968. Global Structure of the Kerr Family of Gravitational Fields, *Phys. Rev. D*, **174**, 1559–1571.

[13] **Hawking, S.W.**, 1975. Particle Creation by Black Holes, *Commun. Math. Phys.*, **43**, 199–220.

[14] **Frolov, V. and Novikov, I.**, 1998. *Physics of Black Holes*, Kluwer Academic Press, Dordrecht.

[15] **Chandrasekhar, S.**, 1983. *The Mathematical Theory of Black Holes*, Clarendon Press, Oxford.

[16] **Kerr, R.P.**, 1963. Gravitational Field of a Spinning Mass as an Example of Algebraically Special Metrics, *Phys. Rev. Lett.*, **11**, 237–238.

[17] **Walker, M. and Penrose, R.**, 1970. On Quadratic First Integrals of the Geodesic Equations for Type [22] Spacetimes, *Commun. Math. Phys.*, **18**, 265–274.

[18] **Teukolsky, S.A.**, 1972. Rotating Black Holes - Separable Wave Equations for Gravitational and Electromagnetic Perturbations, *Phys. Rev. Lett.*, **29**, 1114–1118.

[19] **Bardeen, J.M.**, **Press, W.H. and Teukolsky, S.A.**, 1972. Rotating Black Holes: Locally Nonrotating Frames, Energy Extraction and Scalar Synchrotron Radiation, *Astrophys. J.*, **178**, 347.

[20] **Shapiro, S.L. and Teukolsky, S.A.**, 1983. *Black Holes, White Dwarfs and Neutron Stars*, A Wiley-Interscience Publ., New York.

[21] **Arkani-Hamed, N.**, **Dimopoulos, S. and Dvali, G.**, 1998. The Hierarchy Problem and New Dimensions at a Millimeter, *Phys. Lett. B*, **429**, 263–272.

[22] **Antoniadis, I.**, **Arkani-Hamed, N.**, **Dimopoulos, S. and Dvali, G.**, 1998. New Dimensions at a Millimeter to a Fermi and Superstrings at a TeV, *Phys. Lett. B*, **436**, 257–263.

[23] **Randall, L. and Sundrum, R.**, 1999. A Large Mass Hierarchy from a Small Extra Dimension, *Phys. Rev. Lett.*, **83**, 3370–3373.

[24] **Randall, L. and Sundrum, R.**, 1999. An Alternative to Compactification, *Phys. Rev. Lett.*, **83**, 4690–4693.

[25] **Giddings, S.B. and Thomas, S.**, 2002. High Energy Colliders as Black Hole Factories: The End of Short Distance Physics, *Phys. Rev. D*, **65**, 056010.

[26] **Cavaglia, M.**, 2003. Black hole and brane production in TeV gravity: A review, *Int. J. Mod. Phys. A*, **18**, 1843–1882.

[27] **Shiromizu, T.**, **Maeda, K. and Sasaki, M.**, 2000. The Einstein Equations on the 3-Brane World, *Phys. Rev. D*, **62**, 024012.

[28] **Aliev, A.N. and Gumrukcuoglu, A.E.**, 2004. Gravitational Field Equations on and off a 3-Brane World, *Class. Quant.Grav.*, **21**, 5081–5096.

[29] **Maeda, K. and Torii, T.**, 2003. Covariant gravitational equations on brane world with Gauss-Bonnet term, *Phys. Rev. D*, **69**, 024002.

[30] **Aliev, A.N., Cebeci, H. and Dereli, T.**, 2006. Gravitational field equations in a braneworld with Euler-Poincare term, *Class. Quant. Grav.*, **23**, 591–602.

[31] **Tangherlini, F.R.**, 1963. Schwarzschild field in n dimensions and the dimensionality of space problem, *Nuovo Cimento*, **27**, 636–651.

[32] **Myers, R.C. and Perry, M.J.**, 1986. Black Holes in Higher Dimensional Space-Times, *Ann. Phys. (N.Y.)*, **172**, 304.

[33] **Aliev, A.N. and Frolov, V.P.**, 2004. Five Dimensional Rotating Black Hole in a Uniform Magnetic Field. The Gyromagnetic Ratio, *Phys. Rev. D*, **69**, 084022.

[34] **Aliev, A.N.**, 2006. Rotating black holes in higher dimensional Einstein-Maxwell gravity, *Phys. Rev. D*, **74**, 024011.

[35] **Aliev, A.N.**, 2006. A Slowly rotating charged black hole in five dimensions, *Mod. Phys. Lett. A*, **21**, 751–758.

[36] **Chong, Z.W., Cvetic, M., Lü, H. and N.Pope, C.**, 2005. General Non-Extremal Rotating Black Holes in Minimal Five-Dimensional Gauged Supergravity, *Phys. Rev. Lett.*, **95**, 161301.

[37] **Chamblin, A., Hawking, S.W. and Reall, H.S.**, 2000. Brane world black holes, *Phys. Rev. D*, **61**, 065007.

[38] **Dadhich, N., Maartens, R., Papadopoulos, P. and Rezania, V.**, 2000. Black holes on the brane, *Phys. Lett. B*, **487**, 1–6.

[39] **Aliev, A.N. and Gumrukcuoglu, A.E.**, 2005. Charged rotating black holes on a 3-brane, *Phys. Rev. D*, **71**, 104027.

[40] **Gergely, L.A., Keresztes, Z. and Dwornik, M.**, 2009. Second-order light deflection by tidal charged black holes, *arXiv:gr-qc/0903.1558*.

[41] **Whisker, R.**, 2008. Braneworld Black Holes, *arXiv:gr-qc/0810.1534*.

[42] **Kovar, J., Stuchlik, Z. and Karas, V.**, 2008. Off-equatorial orbits in strong gravitational fields near compact objects, *Class. Quant. Grav.*, **25**, 095011.

[43] **Stuchlik, Z. and Kotrlova, A.**, 2008. Orbital resonances in discs around braneworld Kerr black holes, *arXiv:astro-ph/0812.5066*.

[44] **Chang-Young, E. and Lee, D.**, 2008. Charged Black Holes on DGP Brane, *Phys. Lett. B*, **659**, 58–64.

[45] **Pun, C.S.J., Kovacs, Z. and Harko, T.**, 2008. Thin accretion disks onto brane world black holes, *Phys. Rev. D*, **78**, 084015.

[46] **Harko, T. and Sabau, V.S.**, 2008. Jacobi stability of the vacuum in the static spherically symmetric brane world models, *Phys. Rev. D*, **77**, 104009.

[47] **Liu, L.**, **Wang, B. and Yang, G.**, 2007. The Energy absorption problem of a brane-world black hole, *Phys. Rev. D*, **76**, 064014.

[48] **Shen, J.**, **Wang, B. and Su, R.**, 2006. The Signals from the brane-world black Hole, *Phys. Rev. D*, **74**, 044036.

[49] **Pal, S.**, 2006. Braneworld gravitational collapse from a radiative bulk, *Phys. Rev. D*, **74**, 124019.

[50] **Ovalle, J.**, 2008. Searching exact solutions for compact stars in braneworld: A Conjecture, *Mod.Phys. Lett. A*, **23**, 3247–3263.

[51] **da Rocha, R. and Coimbra-Araujo, C.H.**, 2005. Variation in the luminosity of kerr quasars due to extra dimension in brane randall-sundrum model, *J.Cosmol. Astropart. Phys.*, **0512**, 009.

[52] **da Rocha, R. and Coimbra-Araujo, C.H.**, 2006. Extra dimensions in LHC via mini-black holes: Effective Kerr-Newman brane-world effects, *Phys. Rev. D*, **74**, 055006.

[53] **Majumdar, A.S. and Mukherjee, N.**, 2005. Braneworld black holes in cosmology and astrophysics, *Int. J. Mod. Phys. D*, **14**, 1095.

[54] **Bolton, C.T.**, 1972. Identification of Cygnus X-1 with HDE 226868, *Nature*, **235**, 271–273.

[55] **Mirabel, I.F. and Rodrigues, L.F.**, 1994. A superluminal source in the galaxy, *Nature*, **371**, 46–48.

[56] **Hjellming, R.M. and Rupen, M.P.**, 1995. Episodic ejections of jets by the X-ray transient GRO J1655-40, *Nature*, **375**, 464–468.

[57] **Remillard, R.A. and McClintock, J.E.**, 2006. X-ray Properties of Black-Hole Binaries, *Ann. Rev. Astron. Astrophys.*, **44**, 49–92.

[58] **van der Klis, M.**, 2006. in *Compact Stellar X-ray Sources* vol.39, Cambridge University Press, Cambridge.

[59] **Strohmayer, T.E.**, 2001. Discovery of a Second High Frequency QPO from the Microquasar GRS 1915+105 s, *arXiv:astro-ph/0105338*.

[60] **Strohmayer, T.E.**, 2001. Discovery of a 450 Hz QPO from the Microquasar GRO J1655-40 with RXTE, *arXiv:astro-ph/0104487*.

[61] **Psaltis, D.**, 2004. Measurements of black hole spins and tests of strong-field general relativity, *AIP Conf. Proc.*, **714**, 29–35.

[62] **Aliev, A.N. and Gal'tsov, D.V.**, 1981. Radiation From Relativistic Particle in Nongeodesic Motion in a Strong Gravitational Field, *Gen. Relat. Gravit.*, **13**, 899–912.

[63] **Merloni, A.**, **Vietri, M.**, **Stella, L. and Bini, D.**, 1998. On gravitomagnetic precession around black holes, *arXiv:astro-ph/9811198*.

[64] **Torok, G.**, **Abramowicz, M.A.**, **Kluźniak, W. and Stuchlik, Z.**, 2006. A non-linear resonance model for the black hole and neutron star QPOs: theory supported by observations, *AIP Conf. Proc.*, **861**, 786–793, *arXiv:astro-ph/0603847*.

[65] **Abramowicz, M.A. and Kluźniak, W.**, 2001. A Precise determination of angular momentum in the black hole candidate GRO J1655-40, *Ast.& Ap.*, **379**, L19.

[66] **Abramowicz, M.A. and Kluźniak, W.**, 2003. Interpreting black hole QPOs, *arXiv:astro-ph/0312396*.

[67] **Torok, G.**, **Abramowicz, M.A.**, **Stuchlik, Z. and Sramkova, E.**, 2006. QPOs in microquasars: the spin problem, *arXiv:astro-ph/0610497*.

[68] **DeDeo, S. and Psaltis, D.**, 2004. Testing Strong-field Gravity with Quasiperiodic Oscillation, *arXiv:astro-ph/0405067*.

[69] **Gimon, E.G. and Horava, P.**, 2009. Astrophysical violations of the Kerr bound as a possible signature of string theory, *Phys. Lett. B*, **672**, 299.

[70] **Aliev, A.N.**, **Gal'tsov, D.V. and Petukhov, V.I.**, 1986. Negative Absorption Near a Magnetized Black Hole: Black Hole Masers, *Astr. Space Sci.*, **124**, 137–157.

[71] **Aliev, A.N. and Galt'sov, D.V.**, 1988. Gravitational Effects in the Field of a Central Body Threaded by a Cosmic String, *Sov. Astron. Lett.*, **14**, 48.

[72] **Aliev, A.N. and Gal'tsov, D.V.**, 1989. Magnetized Black Holes, *Sov. Phys. Usp.*, **32**, 75.

[73] **Newman, E.T.**, **Couch, E.**, **Chinnapared, K.**, **Exton, A.**, **Prakash, A. and Torrence, R.**, 1965. Metric of a Rotating Charged Mass, *J. Math. Phys.*, **6**, 918.

[74] **Okazaki, A.**, **Kato, S. and Fukue, J.**, 1987. Global trapped oscillations of relativistic accretion disks, *Publ. Astron. Soc.Japan*, **39**, 457–473.

[75] **Kato, S.**, 1990. Trapped one-armed corrugation waves and QPOs, *Publ. Astron. Soc.Japan*, **42**, 99–113.

[76] **Tsang, D. and Lai, D.**, 2008. Corotational Damping of Diskoseismic C-modes in Black Hole Accretion Discs, *arXiv:astro-ph/0810.1299*.

[77] **McClintock, J.E.**, **Shafee, R.**, **Narayan, R.**, **Remillard, R.A.**, **Davis, S.W. and Li, L.X.**, 2006. The Spin of the Near-Extreme Kerr Black Hole GRS 1915+105, *Astrophys. J.*, **652**, 518–539.

APPENDICES

Appendix A: The Christoffel Symbols

A. THE CHRISTOFFEL SYMBOLS

Using the conventional expression that relates the Christoffel symbols to the derivatives of the metric tensor

$$\Gamma^{\mu}_{\alpha\beta} = \frac{1}{2} g^{\mu\lambda} \left(\frac{\partial g_{\lambda\alpha}}{\partial x^{\beta}} + \frac{\partial g_{\lambda\beta}}{\partial x^{\alpha}} - \frac{\partial g_{\alpha\beta}}{\partial x^{\lambda}} \right), \tag{A.1}$$

we calculate the nonvanishing components of these symbols for the metric (3.4). They are given by

$$\Gamma^{0}_{01} = -\frac{(r^2 + a^2)B}{2\Delta}, \quad \Gamma^{1}_{00} = -\frac{\Delta B}{2\Sigma}, \quad \Gamma^{0}_{02} = -\frac{2Mr - \beta}{2\Sigma^2} a^2 \sin 2\theta,$$

$$\Gamma^{1}_{11} = \frac{\Delta r - (r - M)\Sigma}{\Delta \Sigma}, \quad \Gamma^{0}_{13} = \frac{a \sin^2 \theta}{\Delta} \left[\frac{(r^2 + a^2)B}{2} - \frac{(2Mr - \beta)r}{\Sigma} \right],$$

$$\Gamma^{1}_{22} = -\frac{\Delta r}{\Sigma}, \quad \Gamma^{1}_{12} = -\frac{a^2 \sin 2\theta}{2\Sigma}, \quad \Gamma^{0}_{32} = \frac{2Mr - \beta}{2\Sigma^2} a^3 \sin^2 \theta \sin 2\theta,$$

$$\Gamma^{1}_{33} = -\frac{\Delta}{2\Sigma} \sin^2 \theta \left(2r + Ba^2 \sin^2 \theta \right), \quad \Gamma^{2}_{00} = -\left(\frac{2Mr - \beta}{2\Sigma^2} \right) \frac{a^2 \sin 2\theta}{\Sigma},$$

$$\Gamma^{1}_{03} = \frac{\Delta B}{2\Sigma} a \sin^2 \theta, \quad \Gamma^{2}_{11} = \frac{a^2 \sin 2\theta}{2\Delta \Sigma}, \quad \Gamma^{2}_{12} = \frac{r}{\Sigma}, \quad \Gamma^{2}_{22} = -\frac{a^2 \sin 2\theta}{2\Sigma},$$

$$\Gamma^{2}_{03} = \left(\frac{2Mr - \beta}{2\Sigma^2} \right) \frac{r^2 + a^2}{\Sigma} a \sin 2\theta, \quad \Gamma^{3}_{01} = -\frac{aB}{2\Delta}, \quad \Gamma^{3}_{02} = -\frac{2Mr - \beta}{\Sigma^2} a \cot \theta,$$

$$\Gamma^{2}_{33} = -\frac{\sin 2\theta}{2\Sigma} \left[r^2 + a^2 + \frac{2Mr - \beta}{\Sigma} \left(2 + \frac{a^2 \sin^2 \theta}{\Sigma} \right) a^2 \sin^2 \theta \right],$$

$$\Gamma^{3}_{32} = \frac{\cot \theta}{\Delta} \left[\left(1 - \frac{2Mr - \beta}{\Sigma} \right) \left(r^2 + a^2 + \frac{2Mr - \beta}{\Sigma} a^2 \sin^2 \theta \right) \right.$$

$$\left. + \frac{2Mr - \beta}{\Sigma^2} (r^2 + a^2) a^2 \sin^2 \theta \right],$$

$$\Gamma^{3}_{13} = \frac{r}{\Delta} \left(1 - \frac{2Mr - \beta}{\Sigma} \right) + \frac{a^2 B \sin^2 \theta}{2\Delta}, \tag{A.2}$$

where

$$B = \frac{2M}{\Sigma} \left(1 - \frac{2r^2}{\Sigma} \right) + \frac{2r\beta}{\Sigma^2}. \tag{A.3}$$

CIRRICULUM VITA

Candidate's full name: Pamir TALAZAN

Place and date of birth: İstanbul, 1st of August, 1981

Permanent Address: Şemsettin Günaltay Cd. Afşar Sk. No: 11/9, Kozyatağı, İstanbul

Universities and Colleges attended: In 2000 he started his undergraduate study in Physics Engineering department of İstanbul Technical University. In 2006 he graduated. In 2006 he started the Masters of Science programme for Physics Engineering in İstanbul Technical University.